

# Systematics of single superpartners production at leptonic colliders \*

M. Chemtob and G. Moreau

*Service de Physique Théorique  
CE-Saclay F-91191 Gif-sur-Yvette, Cedex FRANCE*

## Abstract

We examine the effects of the lepton number violating R parity odd superpotential,  $W = \lambda_{ijk} L_i L_j E_k^c$ , on single production of fermion (charginos and neutralinos) and scalar (sleptons and sneutrinos) superpartners at leptonic colliders for center of mass energies up to  $500\text{GeV} - 1\text{TeV}$ . The probability amplitudes for all the five  $2 \rightarrow 2$  body processes:  $l_J^+ l_J^- \rightarrow \tilde{\chi}_1^\pm l_m^\mp$ ,  $\tilde{\chi}_1^0 \nu_m$  ( $\tilde{\chi}_1^0 \tilde{\nu}_m$ ),  $\tilde{l}_m^\mp W^\pm$ ,  $\tilde{\nu}_m Z^0$  ( $\tilde{\nu}_m Z^0$ ),  $\tilde{\nu}_m \gamma$  ( $\tilde{\nu}_m \gamma$ ), and the decays branching ratios for the produced superpartners are calculated at tree level. The rates for all five reactions are proportionnal to  $\lambda_{mJJ}^2$  where  $J = 1, 2$  for  $e^-e^+$  and  $\mu^-\mu^+$  colliders, respectively. A semi-quantitative discussion is presented within a supergravity model assuming grand unification of gauge interactions and universal (flavor independent) soft supersymmetry breaking parameters  $m_0$  (scalars),  $m_{1/2}$  (gauginos) at the unification scale. The predictions obtained for the total and partial rates show that the single production reactions have a good potential of observability at the future  $e^-e^+$  and  $\mu^-\mu^+$  supercolliders. For values of the R parity violating coupling constant of order 0.05, the  $\tilde{\chi}^{\pm,0}$  productions could probe all the relevant intervals for  $\tan\beta$  and  $m_0$  and broad regions of the parameter space for the  $\mu$  (Higgs mixing) and  $m_{1/2}$  parameters ( $|\mu| < 400\text{GeV}$ ,  $m_{1/2} < 240\text{GeV}$ ), while the  $\tilde{\nu}$  and  $\tilde{l}$  productions could probe sneutrinos and sleptons masses up to the kinematical limits ( $m_{\tilde{\nu}} < 500\text{GeV}$ ,  $m_{\tilde{l}} < 400\text{GeV}$ ). Using the hypothesis of a single dominant R parity violating coupling constant, a Monte Carlo events simulation for the reactions,  $l_J^+ l_J^- \rightarrow \tilde{\chi}_1^\pm l_m^\mp$ ,  $\tilde{\chi}_{1,2}^0 \nu_m$ ,  $\tilde{\chi}_{1,2}^0 \tilde{\nu}_m$ , is employed to deduce some characteristic dynamical distributions of the final states.

PACS: 12.60.Jv, 13.10.+q, 14.80.Ly, 13.85.Hd

T98/061..... hep-ph/9807509 .... Phys. Rev. D: DU6463

## 1 Introduction

Should R parity turn out to be an approximate symmetry of the minimal supersymmetric standard model, the truly quantitative tests of such a possibility would have to be sought in high energy colliders physics, as was first emphasized in [1, 2, 3]. The great majority of the existing theoretical studies for the LEP or the Tevatron accelerators physics have focused on signals associated with the LSP (lightest supersymmetric particle) decays and certain rare decays of the standard model particles (gauge [2, 4, 5, 6] or Higgs [2] bosons or top-quark [7]). A few experimental searches have been attempted for  $Z^0$  boson decays [8, 9], for inos decays [10, 11] and also in more general settings [12, 13]. Proceeding one step further, interesting proposals were made recently to explain the so-called ALEPH anomalous four-jets events [14] on the basis of R parity violating decays of neutralinos or charginos [15, 16, 17], squarks [18, 19], sleptons [20] or sneutrinos [21] produced in pairs through the two-body processes,  $e^+e^- \rightarrow \tilde{\chi}^{0,+} \tilde{\chi}^{0,-}$  or  $e^+e^- \rightarrow \tilde{f} \tilde{f}$ . (See [22] for recent updates and lists of references.)

Apart from precursor studies devoted to the HERA collider [23, 24, 25], little consideration was given in the past to single production of supersymmetric particles in spite of the potential interest of a discovery of supersymmetry that might be accessible at lower incident energies. The reason, of course, is the lack of

---

\*Supported by the Laboratoire de la Direction des Sciences de la Matière du Commissariat à l'Energie Atomique

information about the size of the R parity odd coupling constants other than the large number of indirects bounds deduced from low and intermediate energy phenomenology [26]. Therefore, for obvious reasons, the existing single production studies have rather focused on resonant production of sneutrinos, charged sleptons [1, 2, 12, 27, 28, 29, 30, 31, 32] or squarks [3, 23, 27, 28, 29]. The interpretation of the anomalous high  $Q^2$  events recently observed at HERA by the ZEUS [33] and H1 [34] Collaborations, in terms of squark resonant production, has also stimulated a renewed interest in R parity violation phenomenology [35].

The collider physics tests of supersymmetric models without R parity entail an important change in focus with respect to the conventional tests: degraded missing energy, diluted signals, additional background from the minimal supersymmetric standard model interactions and uncertainties from the R parity violation coupling constants compounded with those from the superpartners mass spectra. Our purpose in this work is to discuss semi quantitatively the potential for a discovery and the tests of supersymmetry with  $2 \rightarrow 2$  body single superpartner production. Although several order of magnitudes in rates are lost with respect to the resonant single production, one can dispose here of a rich variety of phenomena with multilepton final states non diagonal in flavor. Besides, one may also test larger ranges of the sneutrino mass since this need not be restricted by the center of mass energy value. Encouraged by the recent developments on R parity violation and by the prospects of high precision measurements at supercolliders [36], we propose to study single production at leptonic (electron and muon) colliders for the set of five  $2 \rightarrow 2$  body reactions,  $l_J^+ l_J^- \rightarrow \tilde{\chi}^\pm l_m^\mp$ ,  $l_J^+ l_J^- \rightarrow \tilde{\chi}^0 \nu_m$  ( $\tilde{\chi}^0 \bar{\nu}_m$ ),  $l_J^+ l_J^- \rightarrow \tilde{l}_m^\mp W^\pm$ ,  $l_J^+ l_J^- \rightarrow \tilde{\nu}_{mL} Z^0$  ( $\tilde{\nu}_{mL} \bar{Z}^0$ ),  $l_J^+ l_J^- \rightarrow \tilde{\nu}_{mL} \gamma$  ( $\tilde{\nu}_{mL} \bar{\gamma}$ ) [ $J = 1, 2$ ], in a more systematic way than has been attempted so far. We limit ourselves to the lowest inos eigenstates. Let us note here that precursor indicative studies of the inos single production reactions were already presented in [37, 38] and that recent discussions concerning the reactions,  $e^\pm \gamma \rightarrow e^\pm \tilde{\nu}$  and  $e^\pm \gamma \rightarrow \tilde{l}^\pm \nu$ , where the photon flux is radiated by one of the two beams, were presented in [39]. We shall restrict our study to the lepton number violating interactions  $L_i L_j E_k^c$  in association with the familiar gauge and Yukawa couplings of the minimal supersymmetric standard model. The final states consist then of multileptons with or without hadronic jets.

This paper contains four sections. In section 2, we present the main formalism for superpartners production cross sections and decay rates. In section 4, based on the supergravity approach to supersymmetry soft breaking parameters, we present numerical results for the total rates and the various branching ratios in wide regions of the parameter space. In section 5, we show results for final states distributions of the processes,  $l_J^+ l_J^- \rightarrow \tilde{\chi}^\pm l_m^\mp$ ,  $\tilde{\chi}^0 \nu$ ,  $\tilde{\chi}^0 \bar{\nu}$ , obtained by means of a Monte Carlo events simulation, using the SUSYGEN routine [40]. In section 6, we state our conclusions.

## 2 General Formalism

Five  $2 \rightarrow 2$  body single production reactions may be observed at leptonic colliders. We shall use the following short hand notation to denote the associated probability amplitudes:

$$\begin{aligned} M(\tilde{\chi}_a^- + l_m^+) &= M(l_J^- + l_J^+ \rightarrow \tilde{\chi}_a^- + l_m^+), \\ M(\tilde{\chi}_a^0 + \bar{\nu}_m) &= M(l_J^- + l_J^+ \rightarrow \tilde{\chi}_a^0 + \bar{\nu}_m), \\ M(\tilde{l}_{mL}^- + W^+) &= M(l_J^- + l_J^+ \rightarrow \tilde{l}_{mL}^- + W^+), \\ M(\tilde{\nu}_m + Z) &= M(l_J^- + l_J^+ \rightarrow \tilde{\nu}_m + Z), \\ M(\tilde{\nu}_m + \gamma) &= M(l_J^- + l_J^+ \rightarrow \tilde{\nu}_m + \gamma), \end{aligned} \quad (1)$$

where  $J = 1, 2$  is a flavor index for the initial state leptons (electrons and muons, respectively), the index  $a$  labels the charginos or neutralinos eigenvalues and the index  $m$  the sleptons or sneutrinos families. Our theoretical framework is the minimal supersymmetric standard model supplemented by the lepton number violating R parity odd superpotential,  $W = \frac{1}{2} \sum_{ijk} \lambda_{ijk} L_i L_j E_k^c$ . This yields the sfermion-fermion Yukawa interactions,

$$L = \frac{1}{2} \sum_{[i \neq j, k]=1}^3 \lambda_{ijk} [\tilde{\nu}_{iL} \bar{e}_{kR} e_{jL} + \tilde{e}_{jL} \bar{e}_{kR} \nu_{iL} + \tilde{e}_{kR}^* \bar{\nu}_{iR}^c e_{jL} - (i \rightarrow j)] + h.c. \quad (2)$$

where the sums labelled by indices,  $i, j, k$ , run over the three leptons and neutrinos families with the condition  $i \neq j$  following from the antisymmetry property,  $\lambda_{ijk} = -\lambda_{jik}$ .

Mass Intervals	Decays	Final State	$\lambda_{m11}$
$m_{\tilde{l}^-} > m_{\tilde{\chi}^-}$ (1) $m_{\tilde{l}^-} < m_{\tilde{\chi}^-}$ (2)	$\bullet \tilde{\chi}^- \rightarrow \bar{\nu}_i \bar{\nu}_j l_k$ $\bullet \tilde{\chi}^- \rightarrow \bar{\nu}_i \tilde{l}_i^- \rightarrow \bar{\nu}_i l_k \bar{\nu}_j$	(A) $l_m^+ l_k^- \cancel{E}$	$l_m^+ e^-$
$m_{\tilde{\nu}} > m_{\tilde{\chi}^-}$ (3) $m_{\tilde{\nu}} < m_{\tilde{\chi}^-}$ (4)	$\bullet \tilde{\chi}^- \rightarrow l_j \bar{l}_k l_i$ $\bullet \tilde{\chi}^- \rightarrow l_i \tilde{\nu}_i \rightarrow l_i l_j \bar{l}_k$	(B) $l_m^+ l_k^+ l_i^- l_j^-$	$l_m^+ l_m^- e^+ e^-$
$m_{\tilde{l}}, m_{\tilde{\nu}} > m_{\tilde{\chi}^-} > m_{\tilde{\chi}^0}$ (5) $m_{\tilde{\chi}^-} > m_{\tilde{l}} > m_{\tilde{\chi}^0}$ (6) $m_{\tilde{\chi}^-} > m_{\tilde{\nu}} > m_{\tilde{\chi}^0}$ (7)	$\bullet \tilde{\chi}^- \rightarrow \tilde{\chi}^0 l_p \bar{\nu}_p \rightarrow l_p \bar{\nu}_p \nu_i l_j \bar{l}_k$ $\bullet \tilde{\chi}^- \rightarrow \bar{\nu}_p \tilde{l}_p^- \rightarrow \bar{\nu}_p l_p \tilde{\chi}^0 \rightarrow l_p \bar{\nu}_p \nu_i l_j \bar{l}_k$ $\bullet \tilde{\chi}^- \rightarrow l_p \tilde{\nu}_p \rightarrow l_p \bar{\nu}_p \tilde{\chi}^0 \rightarrow l_p \bar{\nu}_p \nu_i l_j \bar{l}_k$	(C) $l_m^+ l_p^- l_k^\pm l_i^\mp \cancel{E}$	$l_m^+ l_p^- e^+ e^-$ , $l_m^+ l_p^- e^\pm l_m^\mp$
$m_{\tilde{q}} > m_{\tilde{\chi}^-} > m_{\tilde{\chi}^0}$ (8) $m_{\tilde{\chi}^-} > m_{\tilde{q}} > m_{\tilde{\chi}^0}$ (9)	$\bullet \tilde{\chi}^- \rightarrow \tilde{\chi}^0 q_p \bar{q}_p \rightarrow q_p \bar{q}_p \nu_i l_j \bar{l}_k$ $\bullet \tilde{\chi}^- \rightarrow \bar{q}_p \tilde{q}_p \rightarrow q_p \bar{q}_p \tilde{\chi}^0 \rightarrow q_p \bar{q}_p \nu_i l_j \bar{l}_k$	(D) $l_m^+ l_k^\pm l_i^\mp \cancel{E} + 2jet$	$l_m^+ e^+ e^-$ , $l_m^+ e^\pm l_m^\mp$
$m_{\tilde{\chi}^-} > m_{\tilde{\chi}^0} + m_W$ (10)	$\bullet \tilde{\chi}^- \rightarrow \tilde{\chi}^0 W^- \rightarrow W^- \nu_i l_j \bar{l}_k$	(E) $l_m^+ l_k^\pm l_i^\mp W^- \cancel{E}$	$l_m^+ e^+ e^-$ , $l_m^+ e^\pm l_m^\mp$

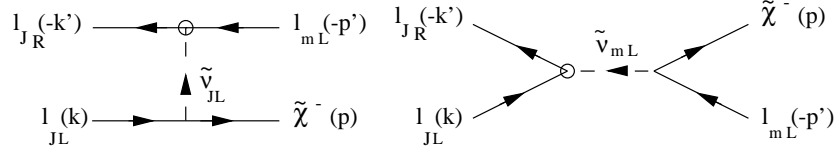
Table 1: The allowed chargino decays for different relative orderings of the superpartners masses. The column fields give the mass intervals, the decay schemes, the final states corresponding to the process,  $l_j^+ l_j^- \rightarrow \tilde{\chi}^- l_m^+$ , with a single dominant coupling constant  $\lambda_{ijk}$  and the leptonic components of the final states in the case of a single dominant coupling constant  $\lambda_{m11}$  [ $m = 2, 3$ ]. The notation  $\cancel{E}$  stands for missing energy associated with neutrinos.

## 2.1 Production Cross Sections

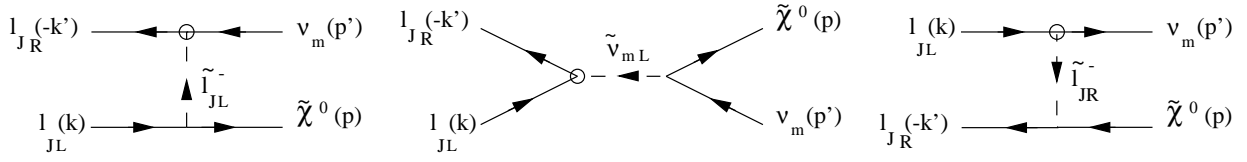
Each of the processes in eq.(1) has a charge conjugate partner such that the transformation between pairs of conjugate amplitudes can be formally described by applying a CP transformation to the S-matrix. The relationship is most easily described at the level of the amplitudes squared obtained after summation over the spins. Because of the simple action of CP on the initial state,  $l_j^+(k) l_j^-(k')$ , it can be seen that the amplitudes for the pairs of charge conjugated processes are related by the substitutions,  $k \leftrightarrow k'$  and  $\lambda_{ijk} \leftrightarrow \lambda_{ijk}^*$ . The tree level probability amplitudes are easily calculated by inspection of the Feynman diagrams given in Fig.1. The formulas for the amplitudes are consigned in Appendix A. A few observations are in order at this point. First, the same configurations of lepton flavor indices, namely,  $\lambda_{mJJ}$  with  $J = 1$ ,  $m = 2, 3$  for  $e^- e^+$  colliders and  $J = 2$ ,  $m = 1, 3$  for  $\mu^- \mu^+$  colliders, occur in all cases. Second, the amplitude for right chirality slepton  $\tilde{l}_{mR}$  production has not been included in the above list of formulas for the reason that this is proportional to the coupling constants  $\lambda_{11m}$  which vanishes by the antisymmetry property,  $\lambda_{ijk} = -\lambda_{jik}$ . Thirdly, all five processes can appear only in a single helicity configuration for the initial fermions (assumed massless), corresponding to identical helicities, namely, either  $l_L^+ l_L^-$  or  $l_R^+ l_R^-$  (recall that physical helicity for antiparticle is opposite to chirality). Lastly, we observe that the relative signs between the  $s, t$  and  $u$  channels contributions are dictated by both the structure of the interaction Lagrangian and the signs of the Wick contractions for fermions. The results for the spin summed squared amplitudes are given by somewhat complicated formulas which we have assembled in Appendix A. We have checked that our formulas for  $\tilde{\chi}^0$  and  $\tilde{\chi}^\pm$  productions agree with the results provided in [37, 38] and [41].

## 2.2 Decays

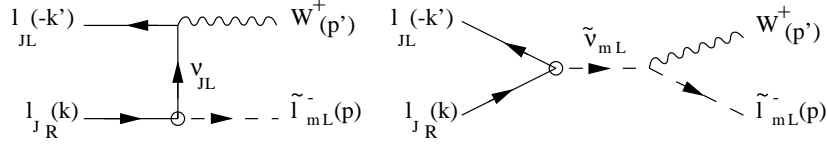
In order to exhibit the possible physical final states, we need to consider the decays of the produced supersymmetric particles, taking into account both the minimal supersymmetric standard model interactions (denoted RPC or R parity conserving) and the R parity odd interactions (denoted RPV or R parity violating).



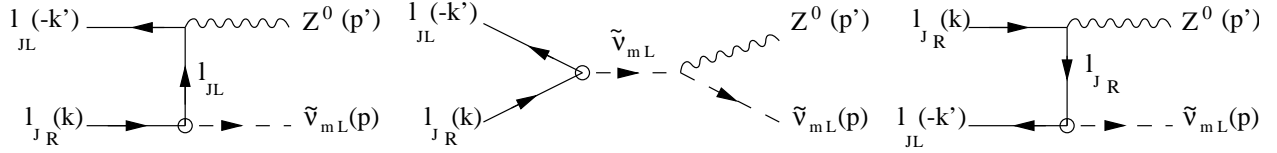
(a)



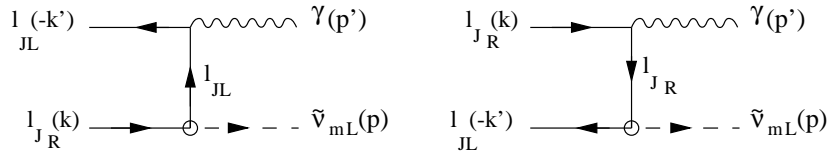
(b)



(c)



(d)



(e)

Figure 1: Feynman diagrams for the processes,  $l_J^+ l_J^- \rightarrow \tilde{\chi}^- l_m^+$  (a),  $l_J^+ l_J^- \rightarrow \tilde{\chi}^0 \nu_m$  (b),  $l_J^+ l_J^- \rightarrow \tilde{l}_{mL}^- W^+$  (c),  $l_J^+ l_J^- \rightarrow \tilde{\nu}_{mL} Z^0$  (d) and  $l_J^+ l_J^- \rightarrow \tilde{\nu}_{mL} \gamma$  (e). The circled vertex correspond to the RPV interaction, with the coupling constant  $\lambda_{mJJ}$ , and the arrows denote flow of momentum.

Mass Intervals	Decays	Final State	$\lambda_{m11}$
$m_{\tilde{\nu}} < m_{\tilde{\chi}^+} \quad (1)$	$\bullet \tilde{\nu}_m \rightarrow l_k \bar{l}_j$	(A) $l_k^- l_j^+ Z^0$	$e^+ e^-$
$m_{\tilde{\nu}} > m_{\tilde{\chi}^+} \quad (2)$	$\bullet \tilde{\nu}_m \rightarrow l_m \tilde{\chi}^+ \rightarrow l_m \bar{l}_i \bar{l}_j l_k$	(B) $l_i^+ l_j^+ l_k^- l_m^- Z^0$	$e^+ e^- l_m^+ l_m^-$
$m_{\tilde{\nu}}, m_{\tilde{l}} > m_{\tilde{\chi}^+} \quad (3)$ $m_{\tilde{\nu}} > m_{\tilde{\chi}^+} > m_{\tilde{l}} \quad (4)$	$\bullet \tilde{\nu}_m \rightarrow l_m \tilde{\chi}^+ \rightarrow l_m \nu_i \nu_j \bar{l}_k$ $\bullet \tilde{\nu}_m \rightarrow l_m \tilde{\chi}^+ \rightarrow l_m \bar{l}_j^+ \nu_j \rightarrow l_m \nu_j \nu_i \bar{l}_k$	(C) $l_k^+ l_m^- \cancel{H} Z^0$	$e^+ l_m^-$
$m_{\tilde{\nu}} > m_{\tilde{\chi}^0} \quad (5)$	$\bullet \tilde{\nu}_m \rightarrow \nu_m \tilde{\chi}^0 \rightarrow \nu_m \nu_i l_j \bar{l}_k$	(D) $l_k^\pm l_i^\mp \cancel{H} Z^0$	$e^+ e^-, e^\pm l_m^\mp$
$m_{\tilde{\nu}} > m_{\tilde{\chi}^+} > m_{\tilde{\chi}^0} \quad (6)$ $m_{\tilde{\nu}} > m_{\tilde{\chi}^+} > m_{\tilde{l}} > m_{\tilde{\chi}^0} \quad (7)$	$\bullet \tilde{\nu}_m \rightarrow \tilde{\chi}^+ l_m \rightarrow l_m \tilde{\chi}^0 \bar{l}_p \nu_p \rightarrow l_m \bar{l}_p \nu_p \nu_i l_j \bar{l}_k$ $\bullet \tilde{\nu}_m \rightarrow \tilde{\chi}^+ l_m \rightarrow l_m \nu_p \bar{l}_p^+ \rightarrow l_m \nu_p \bar{l}_p \tilde{\chi}^0 \rightarrow l_m \nu_p \bar{l}_p \nu_i l_j \bar{l}_k$	(E) $l_p^+ l_m^- l_k^\pm l_i^\mp \cancel{H} Z^0$	$l_p^+ l_m^- e^+ e^-, l_p^+ l_m^- e^\pm l_m^\mp$
$m_{\tilde{\nu}} > m_{\tilde{\chi}^+} > m_{\tilde{\chi}^0} \quad (8)$ $m_{\tilde{\nu}} > m_{\tilde{\chi}^+} > m_{\tilde{q}} > m_{\tilde{\chi}^0} \quad (9)$	$\bullet \tilde{\nu}_m \rightarrow \tilde{\chi}^+ l_m \rightarrow l_m \tilde{\chi}^0 q_p \bar{q}_p \rightarrow l_m q_p \bar{q}_p \nu_i l_j \bar{l}_k$ $\bullet \tilde{\nu}_m \rightarrow \tilde{\chi}^+ l_m \rightarrow l_m \bar{q}_p \tilde{q}_p \rightarrow l_m \bar{q}_p \tilde{q}_p \tilde{\chi}^0 \rightarrow l_m q_p \bar{q}_p \nu_i l_j \bar{l}_k$	(F) $l_m^- l_k^\pm l_i^\mp Z^0 + 2jet$	$l_m^- e^+ e^-, l_m^- e^\pm l_m^\mp$
$m_{\tilde{\nu}} > m_{\tilde{\chi}^+} > m_{\tilde{\chi}^0} + m_W \quad (10)$	$\bullet \tilde{\nu}_m \rightarrow \tilde{\chi}^+ l_m \rightarrow l_m \tilde{\chi}^0 W^+ \rightarrow l_m W^+ \nu_i l_j \bar{l}_k$	(G) $l_m^- l_k^\pm l_i^\mp \cancel{H} W^+ Z^0$	$l_m^- e^+ e^-, l_m^- e^\pm l_m^\mp$

Table 2: The allowed sneutrino decays for different relative orderings of the superpartners masses. The column fields give the mass intervals, the decay schemes, the final states corresponding to the process,  $l_j^+ l_j^- \rightarrow Z^0 \tilde{\nu}_m$ , with a single dominant coupling constant  $\lambda_{ijk}$  and the leptonic components of the final states in the case of a single dominant coupling constant  $\lambda_{m11}$  [ $m = 2, 3$ ]. The notation  $\cancel{H}$  stands for missing energy associated with neutrinos.

A number of hypotheses and approximations, which we list below, will be employed in the evaluation of partial rates.

- 1) Supersymmetric particles decays are assumed to have narrow widths (compared to their masses) and are produced on-shell with negligible spin correlations between the production and decay stages. This allows us to apply the familiar phase space factorisation formula for the production cross sections.
- 2) Spin correlations are neglected at all stages of the cascade decays such that the branching ratios in single or double cascades can be obtained by applying recursively the standard factorisation formula.
- 3) Sleptons belonging to all three families and squarks belonging to the first two families are degenerate in mass. Therefore, for a given decay process as, for instance,  $\tilde{\chi}^- \rightarrow \tilde{\nu}_p l_p$ , either all three generations will be energetically allowed or forbidden. Furthermore, flavor off-diagonal channels such as,  $\tilde{l}_1 \rightarrow \tilde{l}_2 + Z^0, \dots$  are closed.
- 4) The lowest eigenstates of neutralinos  $\tilde{\chi}_a^0$  and charginos  $\tilde{\chi}_a^\pm$  ( $a = 1$ ) are excited in the cascade chains.
- 5) All superpartners decay inside the detector volume. In the presence of broken R parity, the condition for electric charge neutral LSPs to decay inside the detector yields comfortable lower bounds of order  $\lambda > 10^{-7}$  [3, 43].
- 6) Either a single RPV coupling constant is dominant in both the production and decay stages, or a pair of RPV coupling constants are dominant, one in the production stage ( $\lambda_{mJJ}$ ) and the other in the decay stage ( $\lambda_{ijk}$ ). The latter case with two dominant RPV coupling constants may be of interest

Mass Intervals	Decays	Final State	$\lambda_{m11}$
$m_{\tilde{l}^-} < m_{\tilde{\chi}^-}$ (1)	$\bullet \tilde{l}_m^- \rightarrow l_k \bar{\nu}_i$	(A) $l_k^- \cancel{E} W^+$	$e^-$
$m_{\tilde{l}^-} > m_{\tilde{\chi}^-}$ (2)	$\bullet \tilde{l}_m^- \rightarrow \nu_m \tilde{\chi}^- \rightarrow \nu_m l_k \bar{\nu}_j \bar{\nu}_i$	(B) $l_k^- \cancel{E} W^+$	$e^-$
$m_{\tilde{l}^-}, m_{\tilde{\nu}} > m_{\tilde{\chi}^-}$ (3)	$\bullet \tilde{l}_m^- \rightarrow \nu_m \tilde{\chi}^- \rightarrow \nu_m l_j l_k l_i$	(C) $l_k^+ l_i^- l_j^- \cancel{E} W^+$	$e^+ e^- l_m^-$
$m_{\tilde{l}^-} > m_{\tilde{\chi}^-} > m_{\tilde{\nu}}$ (4)	$\bullet \tilde{l}_m^- \rightarrow \nu_m \tilde{\chi}^- \rightarrow \nu_m \tilde{\nu}_i l_i$ $\rightarrow \nu_m l_i l_j \bar{l}_k$		
$m_{\tilde{l}^-} > m_{\tilde{\chi}^0}$ (5)	$\bullet \tilde{l}_m^- \rightarrow l_m \tilde{\chi}^0 \rightarrow l_m \nu_i l_j \bar{l}_k$	(D) $l_m^- l_k^\pm l_i^\mp \cancel{E} W^+$	$l_m^- e^+ e^-$ , $l_m^- e^\pm l_m^\mp$
$m_{\tilde{l}^-} > m_{\tilde{\chi}^-} > m_{\tilde{\chi}^0}$ (6)	$\bullet \tilde{l}_m^- \rightarrow \tilde{\chi}^- \nu_m \rightarrow \nu_m \tilde{\chi}^0 l_p \bar{\nu}_p$ $\rightarrow \nu_m l_p \bar{\nu}_p \nu_i l_j \bar{l}_k$	(E) $l_p^- l_k^\pm l_i^\mp \cancel{E} W^+$	$l_p^- e^+ e^-$ , $l_p^- e^\pm l_m^\mp$
$m_{\tilde{l}^-} > m_{\tilde{\chi}^-} > m_{\tilde{\nu}} > m_{\tilde{\chi}^0}$ (7)	$\bullet \tilde{l}_m^- \rightarrow \tilde{\chi}^- \nu_m \rightarrow \nu_m l_p \bar{\nu}_p$ $\rightarrow \nu_m l_p \bar{\nu}_p \tilde{\chi}^0 \rightarrow \nu_m l_p \bar{\nu}_p \nu_i l_j \bar{l}_k$		
$m_{\tilde{l}^-} > m_{\tilde{\chi}^-} > m_{\tilde{\chi}^0}$ (8)	$\bullet \tilde{l}_m^- \rightarrow \tilde{\chi}^- \nu_m \rightarrow \nu_m \tilde{\chi}^0 q_p \bar{q}_p$ $\rightarrow \nu_m q_p \bar{q}_p \nu_i l_j \bar{l}_k$	(F) $l_k^\pm l_i^\mp \cancel{E} W^+ + 2jet$	$e^+ e^-$ , $e^\pm l_m^\mp$
$m_{\tilde{l}^-} > m_{\tilde{\chi}^-} > m_{\tilde{q}} > m_{\tilde{\chi}^0}$ (9)	$\bullet \tilde{l}_m^- \rightarrow \tilde{\chi}^- \nu_m \rightarrow \nu_m \bar{q}_p \tilde{q}_p$ $\rightarrow \nu_m \bar{q}_p q_p \tilde{\chi}^0 \rightarrow \nu_m \bar{q}_p q_p \nu_i l_j \bar{l}_k$		
$m_{\tilde{l}^-} > m_{\tilde{\chi}^-} > m_{\tilde{\chi}^0} + m_W$ (10)	$\bullet \tilde{l}_m^- \rightarrow \tilde{\chi}^- \nu_m \rightarrow \nu_m \tilde{\chi}^0 W^-$ $\rightarrow \nu_m W^- \nu_i l_j \bar{l}_k$	(G) $l_k^\pm l_i^\mp W^- \cancel{E} W^+$	$e^+ e^-$ , $e^\pm l_m^\mp$

Table 3: The allowed slepton decays for different relative orderings of the superpartners masses. The column fields give the mass intervals, the decay schemes, the final states corresponding to the process,  $l_j^+ l_j^- \rightarrow W^+ \tilde{l}_m^-$ , with a single dominant coupling constant  $\lambda_{ijk}$  and the leptonic components of the final states in the case of a single dominant coupling constant  $\lambda_{m11}$  [ $m = 2, 3$ ]. The notation  $\cancel{E}$  stands for missing energy associated with neutrinos.

since strong bounds on quadratic products exist only for a few family configurations. The strongest bounds arise from the  $\mu \rightarrow 3e$  decay [42]:  $\lambda_{p11}\lambda_{p12} < 6.5 \cdot 10^{-7}$ ,  $\lambda_{p21}\lambda_{p11} < 6.5 \cdot 10^{-7}$  [ $p = 2, 3$ ], while other quadratic product bounds are of order  $10^{-3}, 10^{-4}$ . Besides, as long as the coupling constant  $\lambda$ , which controls the RPV decays, is small in comparison with the gauge coupling constants but not very much smaller (so that the LSP decays inside the detector), then the branching ratio will depend weakly on  $\lambda$  since the last stage of the decay chain (LSP decay) is independent of  $\lambda$ .

- 7) The widths for the decays with four and higher body final states are neglected, such as those which occur in slepton (sneutrino) decays for,  $m_{\tilde{\chi}^-}, m_{\tilde{\chi}^0} > m_{\tilde{l}^-}$  ( $m_{\tilde{\chi}^-}, m_{\tilde{\chi}^0} > m_{\tilde{\nu}}$ ), mediated by virtual charginos or neutralinos, namely,  $\tilde{l}_m^- \rightarrow \nu_m l_k \bar{\nu}_j \bar{\nu}_i$  and  $\tilde{l}_m^- \rightarrow l_m \bar{l}_k l_j \nu_i$  ( $\tilde{\nu}_m \rightarrow l_m l_k \bar{l}_j \bar{l}_i$  and  $\tilde{\nu}_m \rightarrow \nu_m \bar{l}_k l_j \nu_i$ ).
- 8) A supergravity model for the soft supersymmetry breaking parameters is used where, generically,  $\tilde{\chi}_1^0$  is the LSP.

The consideration of the various order relations in the superpartners mass spectrum leads to a list of decay schemes for the initially produced superparticles. These are displayed in Tables 1, 2 and 3, for  $\tilde{\chi}^\pm$ ,  $\tilde{\nu}_L$  and  $\tilde{l}_L$ , respectively. The signals for the  $\tilde{\chi}_1^0$  decays are very few in number and will be discussed separately in section 4.2.1. Some comments on these tables are in order. Except for hadronic dijet pairs from the decay processes,  $\tilde{\chi}^\pm \rightarrow \tilde{\chi}^0 \bar{q} q'$ , all other final particles will consists of multileptons and missing energy associated with neutrinos. In the hypothesis of a single dominant RPV coupling constant in the decays stage, one can deduce the various final states flavor configurations by an inspection of the tables (cf. tables captions). The produced  $\tilde{\chi}^0$ ,  $\tilde{\chi}^\pm$ ,  $\tilde{\nu}$ ,  $\tilde{l}^\pm$  will decay according to cascade schemes dictated by the superpartners mass spectrum. It is important to distinguish the direct RPV induced decays:  $\tilde{\chi}^- \rightarrow \bar{\nu}_i \bar{\nu}_j l_k$ ,  $\tilde{\chi}^- \rightarrow l_i l_j \bar{l}_k$ ,  $\tilde{\chi}^0 \rightarrow \nu_i l_j \bar{l}_k$ ,  $\tilde{\chi}^0 \rightarrow \bar{\nu}_i l_j l_k$ ,  $\tilde{\nu}_i \rightarrow l_k \bar{l}_j$ ,  $\tilde{l}_{kR}^- \rightarrow l_j \nu_i$ , and  $\tilde{l}_{jL}^- \rightarrow l_k \bar{\nu}_i$ , from the indirect RPC induced decays:  $\tilde{l}_L^- \rightarrow \tilde{\chi}^- \bar{\nu}$ ,  $\tilde{\nu}_L \rightarrow \tilde{\chi}^+ l$ ,  $\tilde{l}_{L,R}^- \rightarrow \tilde{\chi}^0 l$ ,  $\tilde{\nu}_L \rightarrow \tilde{\chi}^0 \nu$ ,  $\tilde{\chi}^0 \rightarrow \tilde{l}^- \bar{l}$ ,  $\tilde{\chi}^0 \rightarrow l \bar{l}^+$ ,  $\tilde{\chi}^- \rightarrow \tilde{l}^- \bar{\nu}$ ,  $\tilde{\chi}^- \rightarrow l \tilde{\nu}$  and  $\tilde{\chi}^\pm \rightarrow \tilde{\chi}^0 W^\pm$  for two-body final states and,  $\tilde{\chi}^- \rightarrow \tilde{\chi}^0 f \bar{f}$  ( $f$ =leptons or quarks), for three-body final states. All the formulas needed to evaluate the partial decay widths are quoted in the Appendix B. As can be seen from Tables 1,2,3, a given final state can arise from different processes,

depending on the relative orderings of the masses. A reaction chain occurring through an intermediate particle which is produced on-shell leads obviously to the same final state when the production of this particle is kinematically forbidden and it must then occur through a virtual intermediate state. In the approximation of family degenerate sleptons, sneutrinos and squarks, the index  $p$  in the tables runs over the three generations. A single exception is the hadronic decay,  $\tilde{\chi}^\pm \rightarrow \tilde{\chi}^0 u_p \bar{d}_p (\tilde{\chi}^0 d_p \bar{u}_p)$ , which is restricted to the first two families because of the large top-quark mass.

Another subtle point concerns the multiplicity of a given signal, namely, the number of different configurations which can lead to the same final state. Due to the antisymmetry property of  $\lambda_{ijk}$ , the final states from chargino RPV decays (cf. A and B in Table 1) have a multiplicity of two. The reason is that these decays proceed through the exchanges of the sleptons (or sneutrinos) in families  $i$  and  $j$ , for a given  $\lambda_{ijk}$ . This fact is already accounted for in the virtual  $\tilde{\chi}^\pm$  three-body decays (A(1), B(1), Table 1), but must be put by hand in the  $\tilde{\chi}^\pm$  cascade decays proceeding through the on-shell production of sleptons or sneutrinos which decay subsequently (A(2), B(2), Table 1).

To get a better understanding of the interplay between RPC and RPV decays, it is helpful to note that the branching ratios can be written formally as,  $B_D = \frac{\lambda^2}{c g^2 + \lambda^2}$ , for direct decays and,  $B_I = \frac{g^2 B}{c_0 g^2 + \lambda^2}$ , for two-stages indirect decays, where  $B = \frac{\lambda^2}{c g^2 + \lambda^2}$  is the LSP branching ratio,  $\lambda$  and  $g$  are symbolic notations for the RPV and RPC coupling constants and  $c, c_0$  are calculable constants. Of course,  $B = 1$ , if the last decaying particle is the LSP, which is the generic case. For values of the RPV coupling constants small with respect to the gauge coupling constants ( $\lambda \leq 0.05$ ), namely,  $g^2 \gg \lambda^2$ , the dependence on  $\lambda$  of the indirect decays branching ratios is weak and we have,  $B_I \gg B_D$ . For large enough RPV coupling constant (for example,  $\lambda = 0.1$ ) or for suppressed indirect decays (due for example to kinematical reasons), the direct decays may become competitive and both the direct and indirect branching ratios depend strongly on  $\lambda$ .

### 3 The model and its parameter space

We shall develop the study of single superpartner production within a non minimal supergravity framework, assuming the existence of a grand unified gauge theory and of family universal boundary conditions on the supersymmetry breaking parameters. The renormalization group improved classical spectrum of the scalar superpartners is determined in principle by the full set of soft supersymmetry breaking parameters at the unification scale,  $M_X$ , namely,  $m_0$  (common scalars mass),  $m_{1/2}$  (common gauginos mass),  $A$  (trilinear Yukawa interactions),  $B_\mu$  (bilinear Higgs interaction); by the parameters  $\tan \beta = \frac{v_u}{v_d} = \frac{\langle H_u \rangle}{\langle H_d \rangle}$  and  $\mu(t)$ , where  $t$  denotes the running scale; and by the gauge coupling constants,  $g_a(t)$ , along with fermions masses,  $m_f^2(t)$ . If one neglects the Yukawa interactions of quarks and leptons with the Higgs bosons, then the running masses of all sfermions remain family degenerate down to the electroweak breaking scale where they are described by the familiar additive formula,

$$m_{\tilde{f}}^2(t) = m_f^2(t) + m_0^2 + c_f(t) m_{1/2}^2 \pm m_{\tilde{Z}^0}^2 \cos(2\beta) (T_3^f - Q^f x_W), \quad (3)$$

where  $c_f(t)$  are calculable coefficients depending on the gauge interactions parameters and the last term represents the D-term contribution, the upper and lower sign being for the left and right chirality sfermions, respectively. The most relevant Yukawa coupling constants, namely, those of the third family of up-quarks or, for large  $\tan \beta$ , of d-quarks and leptons, are expected to induce downwards shifts for the third family squarks (up and down) and sleptons, which depend non trivially on the parameters  $A$  and  $\mu$ . In this work, we shall restrict consideration to the simple case of family independent running masses and employ the approximate representation in eq.(3) with the numerical values quoted in [44]. Note that the total rates do not depend on the squarks masses and, as already remarked in section 2.2, the third families of squarks are not considered in the cascade decays. The charginos and neutralinos classical mass spectra are determined by the subset of parameters:  $M_1(t)$ ,  $M_2(t)$ ,  $\mu(t)$  and  $\tan \beta$ . For fixed  $m_{1/2}$ , the solution of the one loop renormalization group equations is given explicitly by,  $m_{1/2} = (1 - \beta_a t) M_a(t)$ , where  $t = \log(\frac{M_X^2}{Q^2})$ ,  $Q$  denoting the running scale,  $\beta_a = \frac{g_X^2 b_a}{(4\pi)^2}$ ,  $b_a = (3, -1, -11)$  with  $a = (3, 2, 1)$ , corresponding to the beta functions parameters for the gauge group factors,  $SU(3)$ ,  $SU(2)_L$ ,  $U(1)_Y$ , and  $g_X$  is the coupling constant at unification scale. Note that the wino and bino masses are related as,  $M_1(t) = \frac{5}{3} M_2(t) \tan^2 \theta_W$ . It is useful here to comment on the relation of our framework with the so-called

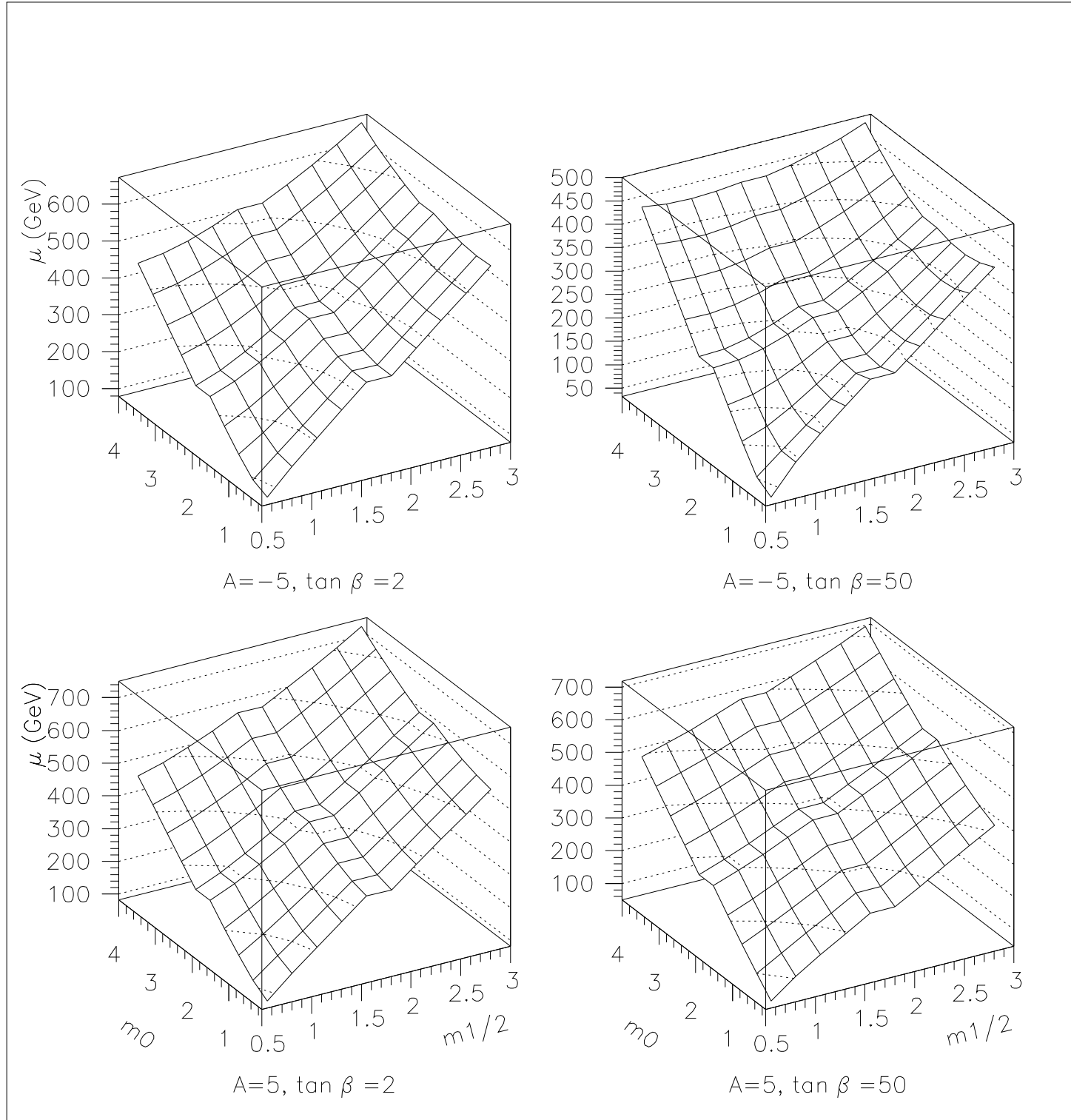


Figure 2: The solution  $\mu(t_Z)$ , at scale  $m_Z$ , for the electroweak symmetry radiative breaking equations, at running top-quark mass,  $m_t(m_t) = 171$  GeV ( $m_t^{\text{pole}} = 180$  GeV), is plotted as a function of  $\frac{m_0}{100\text{GeV}}$  and  $\frac{m_{1/2}}{100\text{GeV}}$  for four values of the pair of parameters,  $A$  and  $\tan \beta$ .



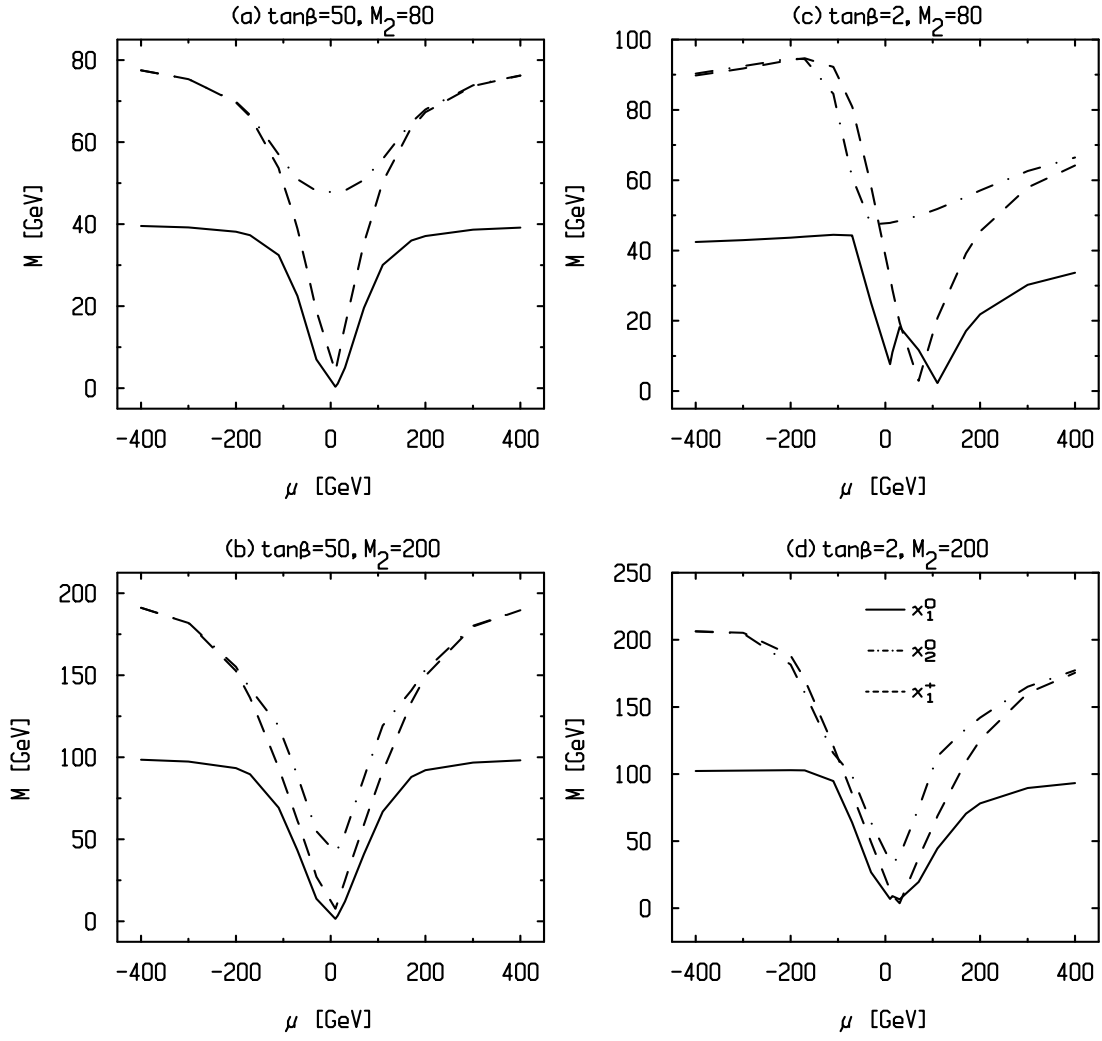


Figure 3: Mass spectrum for the chargino  $\tilde{\chi}_1^\pm$  and the first two lowest mass neutralinos,  $\tilde{\chi}_1^0$  and  $\tilde{\chi}_2^0$ , as a function of  $\mu$ . Four choices of the parameters,  $\tan\beta$  and  $M_2$  (in GeV), are used, as indicated on top of each window.

minimal supergravity framework in which one assumes a constrained parameter space compatible with electroweak symmetry breaking. Let us follow here the so-called ambidextrous minimal supergravity approach [45], where one chooses  $[m_0, m_{1/2}, A, \text{sign}(\mu), \tan\beta]$  as the free parameters set and derives  $\mu(t_Z), B_\mu(t_Z)$ , at the electroweak symmetry breaking scale,  $t_Z = \ln M_X^2/m_Z^2$ , through the minimisation equations for the Higgs bosons potential. For fixed  $m_0, m_{1/2}$  and  $\tan\beta$ , varying  $A$  will let the parameter  $\mu(t_Z)$  span finite intervals of relatively restricted sizes. In figure 2, we give results of a numerical resolution of the renormalization group equations which show the variation of  $|\mu(t_Z)|$  as a function of  $m_0$  and  $m_{1/2}$ , and also exhibit its dependence on  $A$ . Note that the equations admit the symmetry,  $\mu(t_Z) \rightarrow -\mu(t_Z)$ . Observing that  $\mu(t_Z)$  is typically a monotonous increasing function of  $A$ , we see from Fig.2 that the corresponding incremental increase,  $\delta\mu(t_Z)/\mu(t_Z)$ , as one spans the wide interval,  $A \in [-5, +5]$ , is small and of order 20%.

In the infrared fixed point approach for the top-quark Yukawa coupling,  $\tan\beta$  is fixed (up to the ambiguity associated with large or low  $\tan\beta$  solutions) in terms of the top-quark mass,  $m_t = C \sin\beta$ , with,  $C \simeq 190 - 210 \text{ GeV}$ , for,  $\alpha_3(m_{Z^0}) = 0.11 - 0.13$  [46]. The dependence on  $A$  of the electroweak constraint also becomes very weak, so that  $\mu(t_Z)$  is a known function of  $m_0, m_{1/2}$  and  $\tan\beta$  [46]:

$$\mu^2 + \frac{m_Z^2}{2} = m_0^2 \frac{1 + 0.5 \tan^2 \beta}{\tan^2 \beta - 1} + m_{1/2}^2 \frac{0.5 + 3.5 \tan^2 \beta}{\tan^2 \beta - 1}. \quad (4)$$

In section 4.2, we will discuss results for the branching ratios in this constrained model. The total rates are not affected in any significant way by which version of the supergravity models is used, since, as we will see, their dependence on  $\tan\beta$  and  $m_0$  turns out to be smooth.

The main uncertain inputs are the superpartners mass spectrum and the coupling constants  $\lambda_{ijk}$ . To survey the characteristic properties of single production over a broad region of parameter space, we found it convenient to consider a continuous interval of variation for  $\mu(t_Z)$ , namely,  $\mu(t_Z) \in [-400, +400] \text{ GeV}$ , while choosing suitable discrete values for the other parameters:  $M_2(t_Z) = 50, 80, 100, 150, 200 \text{ GeV}$ ,  $m_0 = 20, 50, 150 \text{ GeV}$  and  $\tan\beta = 2, 50$ . We shall set the unification scale at  $M_X = 2 \cdot 10^{16} \text{ GeV}$  and the running scale at  $Q^2 = m_Z^2$ . For definiteness, we choose the coupling constant, which controls the size of the production cross section, at the reference value:  $\lambda_{mJJ} = 0.05$ . This is the strongest bound for a slepton mass of  $100 \text{ GeV}$  [26]. The dependence of integrated total rates on  $\lambda_{mJJ}$  is then given by a simple rescaling  $(\frac{\lambda_{mJJ}}{0.05})^2$  but that of branching ratios on  $\lambda_{ijk}$  (which may or may not be identified with  $\lambda_{mJJ}$ ) is more complicated because of the interplay between the RPC and RPV contributions which add up in the total decay widths. The reference value used here,  $\lambda_{ijk} = 0.05$ , is also an interesting borderline value since below this value the dependence of branching fractions on  $\lambda_{ijk}$  becomes negligible in generic cases.

It will prove helpful in the following discussion to keep within sight the spectrum for the low-lying inos. We display in Figure 3 the results obtained by solving numerically the eigenvalues problem for the charginos and neutralinos mass matrices. Recall the current experimental bounds [47],  $m_{\tilde{\chi}_1^0} > 23 \text{ GeV}$ ,  $m_{\tilde{\chi}_1^\pm} > 45 \text{ GeV}$ ,  $m_{\tilde{\nu}} > 37.1 \text{ GeV}$  and  $m_{\tilde{l}} > 45 \text{ GeV}$ . The following remarks about Figure 3 will prove relevant for the discussion on branching fractions: (i) The symmetry of the spectra under,  $\mu \leftrightarrow -\mu$ , is spoilt at low  $\tan\beta$  as can be seen on the explicit expression for the inos masses in [48]; (ii) The mass differences  $\tilde{\chi}^+ - \tilde{\chi}^0$  increase with  $|\mu|$  with a steep rise appearing at,  $\mu = M_2$ , the borderline between the Higgsino and gaugino dominant regimes; (iii) The spacings  $\tilde{\chi}_2^0 - \tilde{\chi}_1^0$  and  $\tilde{\chi}_1^+ - \tilde{\chi}_1^0$  decrease in magnitudes, relatively to the  $\tilde{\chi}_1^0$  mass, with increasing  $M_2$ . Although we show here the results for  $\tilde{\chi}_2^0$  mass, the interesting possibility of exciting the second neutralino  $\tilde{\chi}_2^0$  is not considered in the subsequent discussion.

## 4 Results and discussion

### 4.1 Total production rates

The total production rates are evaluated by taking the angular integral,  $\sigma = \int_{-x_m}^{+x_m} \frac{d\sigma}{dx} dx$ ,  $[x = \cos\theta]$ , over the differential cross sections which are given explicitly in eqs.(A.2)-(A.6) in Appendix A. To follow the usual practice we shall set an angular cut-off to account for the poor detection condition along the beam pipe:  $170^\circ > \theta_m > 10^\circ$ , corresponding to  $x_m = \cos\theta_m = 0.9848$ .

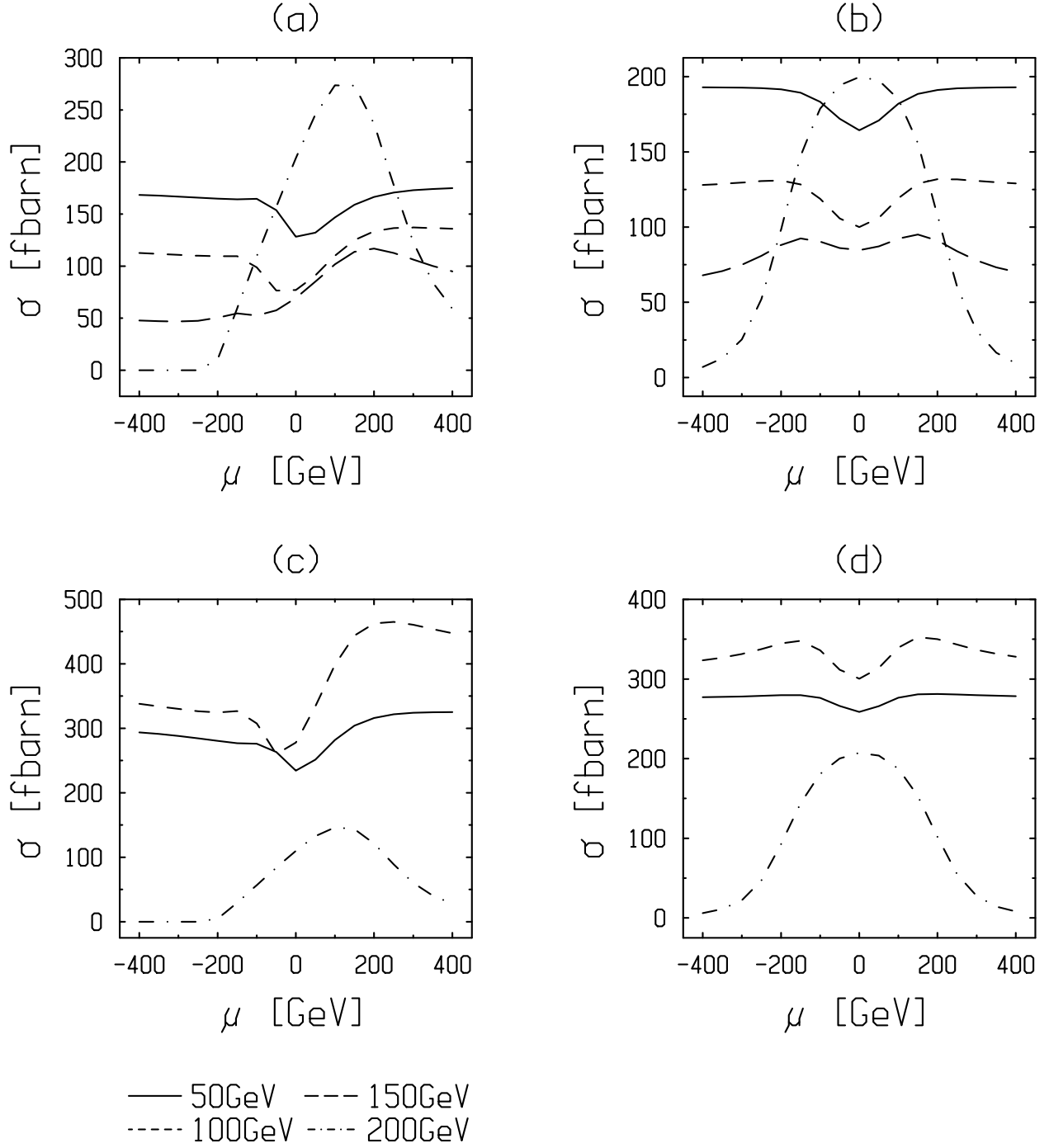


Figure 4: The integrated cross sections for the process,  $l_J^+ l_J^- \rightarrow \tilde{\chi}_1^- l_m^+$ , at a center of mass energy of 200 GeV, are shown as a function of  $\mu$  for discrete choices of the remaining parameters: (a)  $\tan \beta = 2$ ,  $m_0 = 50 \text{ GeV}$ , (b)  $\tan \beta = 50$ ,  $m_0 = 50 \text{ GeV}$ , (c)  $\tan \beta = 2$ ,  $m_0 = 150 \text{ GeV}$  and (d)  $\tan \beta = 50$ ,  $m_0 = 150 \text{ GeV}$ , with  $\lambda_{mJJ} = 0.05$ . The windows conventions are such that  $\tan \beta = 2, 50$  horizontally and  $m_0 = 50, 150 \text{ GeV}$  vertically. The different curves refer to the values of  $M_2$  of 50 GeV (continuous line), 100 GeV (dot-dashed line), 150 GeV (dashed line) and 200 GeV (dotted line), as indicated at the bottom of the figure.

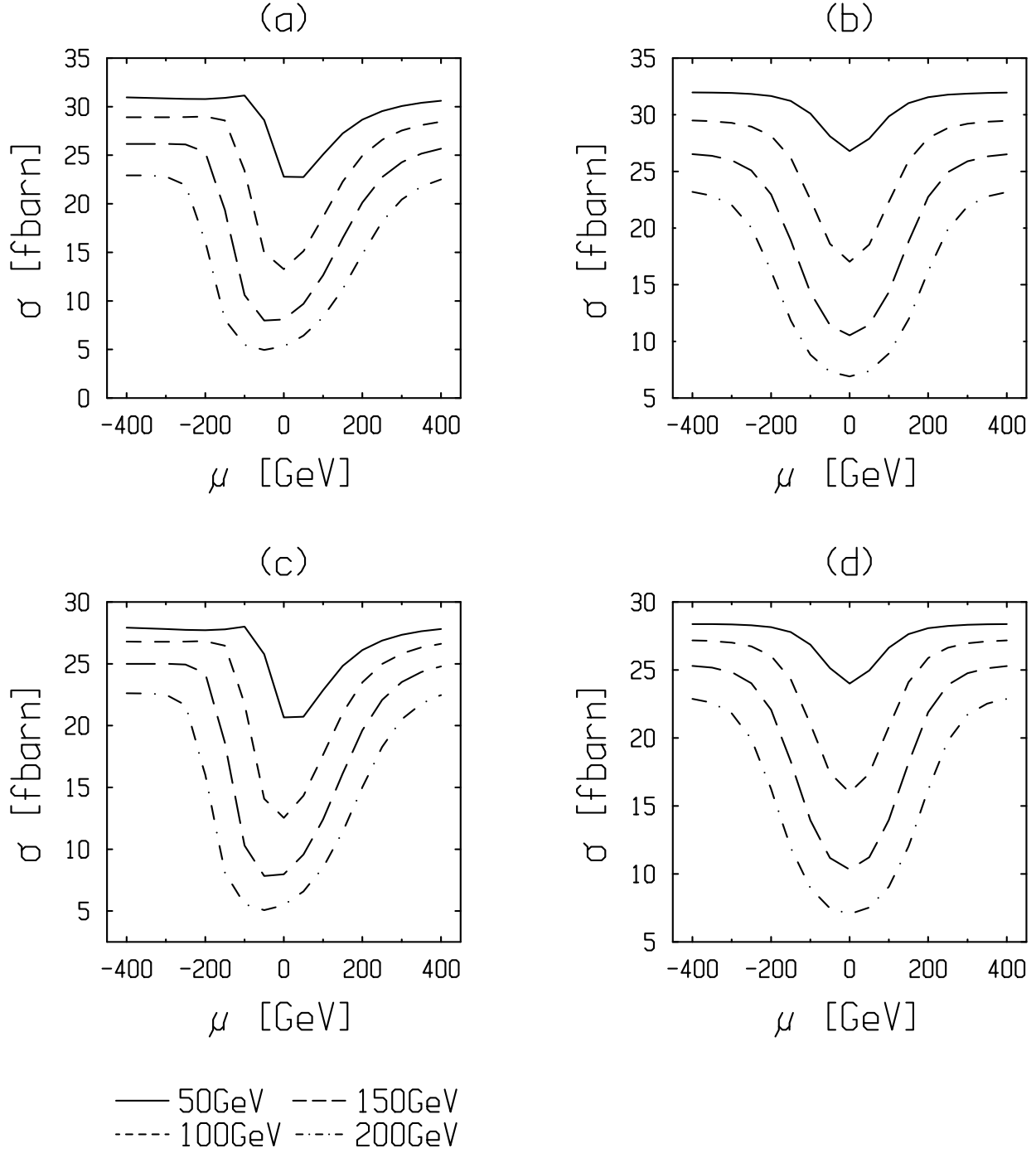


Figure 5: The integrated cross sections for the process,  $l_J^+ l_J^- \rightarrow \tilde{\chi}_1^- l_m^+$ , at a center of mass energy of 500 GeV, are shown as a function of  $\mu$  for discrete choices of the remaining parameters: (a)  $\tan \beta = 2$ ,  $m_0 = 50 \text{ GeV}$ , (b)  $\tan \beta = 50$ ,  $m_0 = 50 \text{ GeV}$ , (c)  $\tan \beta = 2$ ,  $m_0 = 150 \text{ GeV}$  and (d)  $\tan \beta = 50$ ,  $m_0 = 150 \text{ GeV}$ , with  $\lambda_{mJJ} = 0.05$ . The windows conventions are such that  $\tan \beta = 2, 50$  horizontally and  $m_0 = 50, 150 \text{ GeV}$  vertically. The different curves refer to the values of  $M_2$  of 50 GeV (continuous line), 100 GeV (dot-dashed line), 150 GeV (dashed line) and 200 GeV (dotted line), as indicated at the bottom of the figure.

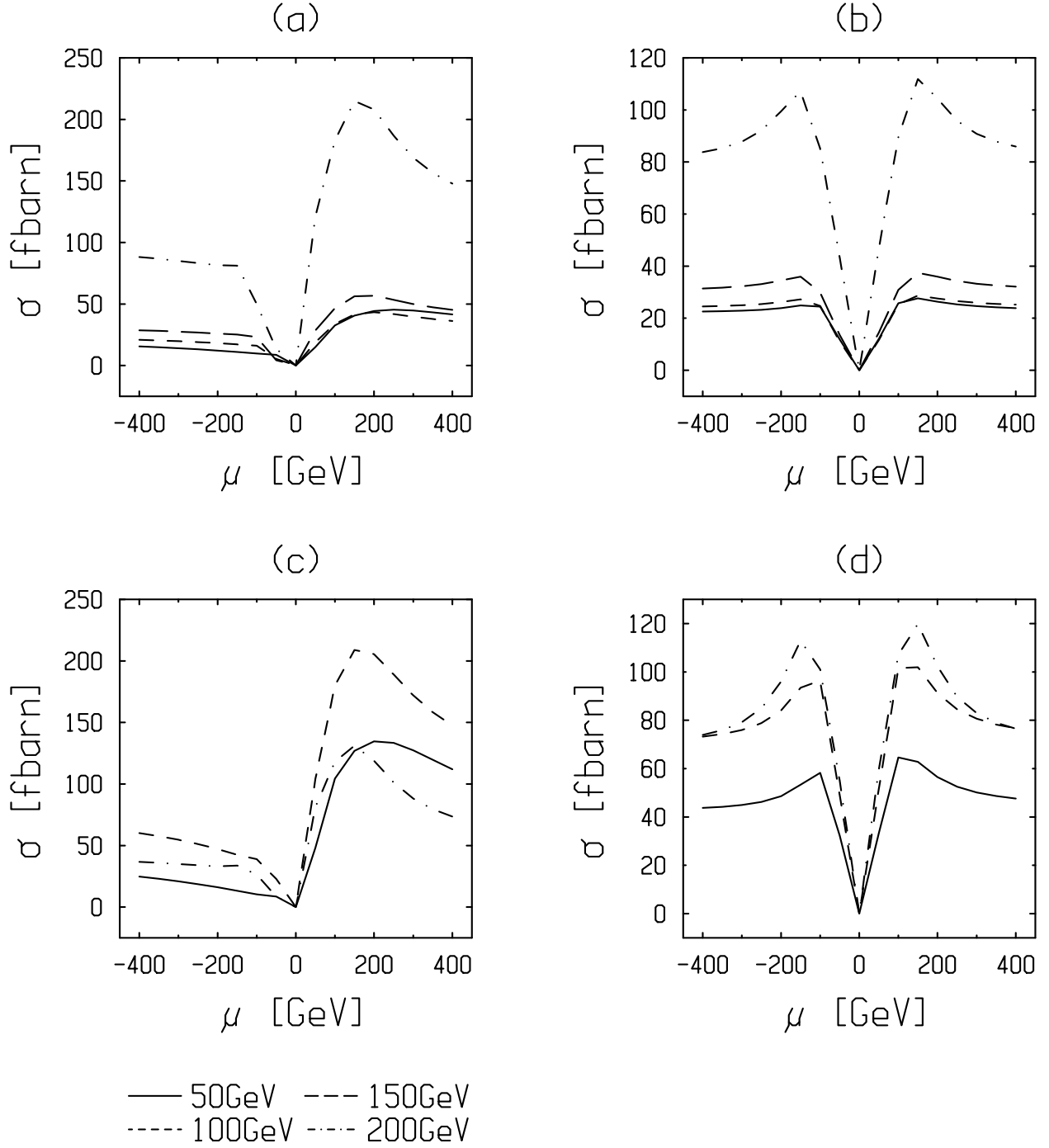


Figure 6: The integrated cross sections for the process,  $l_J^+ l_J^- \rightarrow \tilde{\chi}_1^0 \bar{\nu}_m$ , at a center of mass energy of 200 GeV, are shown as a function of  $\mu$  for discrete choices of the remaining parameters: (a)  $\tan \beta = 2$ ,  $m_0 = 50$  GeV, (b)  $\tan \beta = 50$ ,  $m_0 = 50$  GeV, (c)  $\tan \beta = 2$ ,  $m_0 = 150$  GeV and (d)  $\tan \beta = 50$ ,  $m_0 = 150$  GeV, with  $\lambda_{mJJ} = 0.05$ . The windows conventions are such that  $\tan \beta = 2, 50$  horizontally and  $m_0 = 50, 150$  GeV vertically. The different curves refer to the values of  $M_2$  of 50 GeV (continuous line), 100 GeV (dot-dashed line), 150 GeV (dashed line) and 200 GeV (dotted line), as indicated at the bottom of the figure.

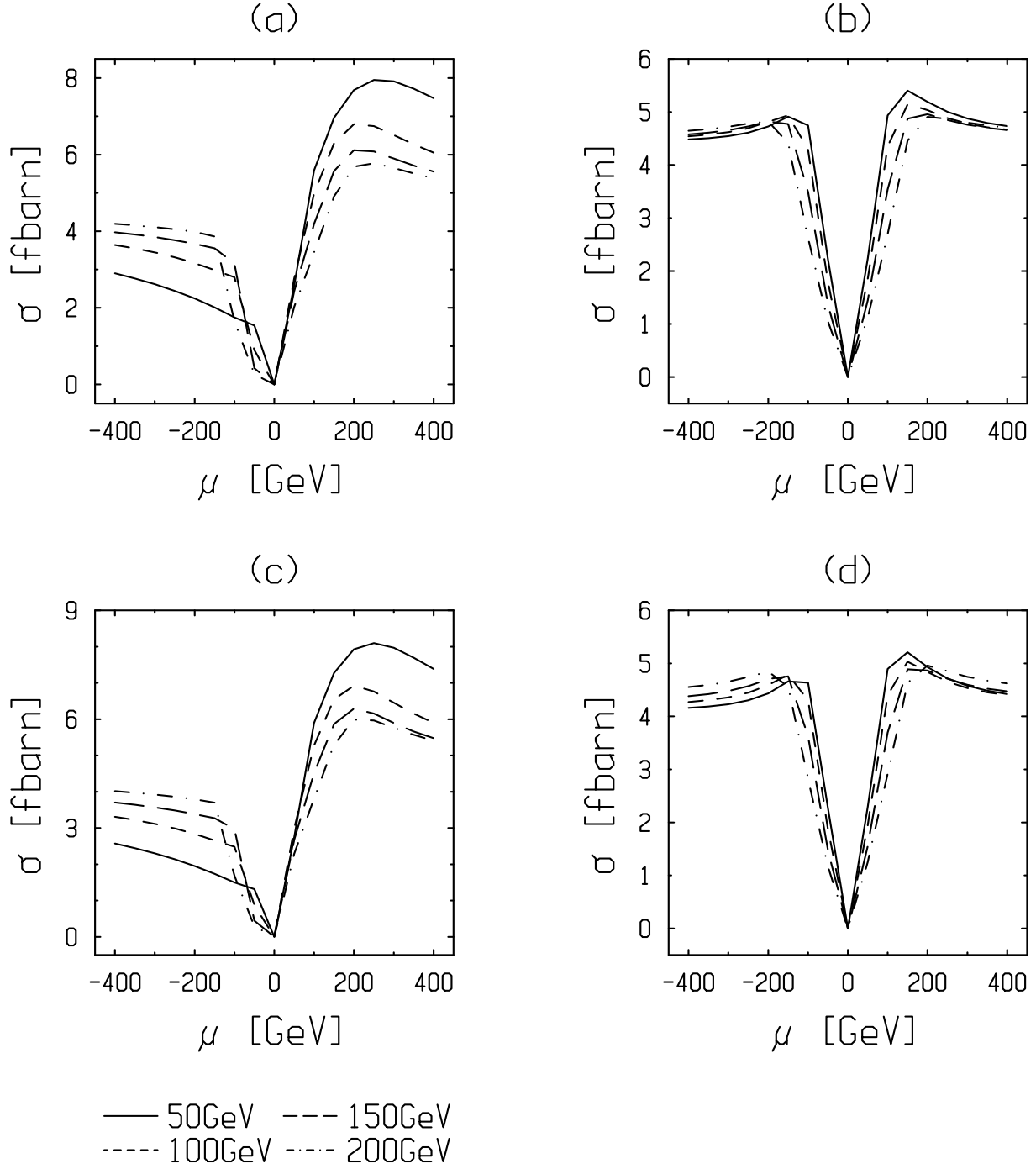


Figure 7: The integrated cross sections for the process,  $l_J^+ l_J^- \rightarrow \tilde{\chi}_1^0 \bar{\nu}_m$ , at a center of mass energy of 500 GeV, are shown as a function of  $\mu$  for discrete choices of the remaining parameters: (a)  $\tan \beta = 2$ ,  $m_0 = 50 \text{ GeV}$ , (b)  $\tan \beta = 50$ ,  $m_0 = 50 \text{ GeV}$ , (c)  $\tan \beta = 2$ ,  $m_0 = 150 \text{ GeV}$  and (d)  $\tan \beta = 50$ ,  $m_0 = 150 \text{ GeV}$ , with  $\lambda_{mJJ} = 0.05$ . The windows conventions are such that  $\tan \beta = 2, 50$  horizontally and  $m_0 = 50, 150 \text{ GeV}$  vertically. The different curves refer to the values of  $M_2$  of 50 GeV (continuous line), 100 GeV (dot-dashed line), 150 GeV (dashed line) and 200 GeV (dotted line), as indicated at the bottom of the figure.

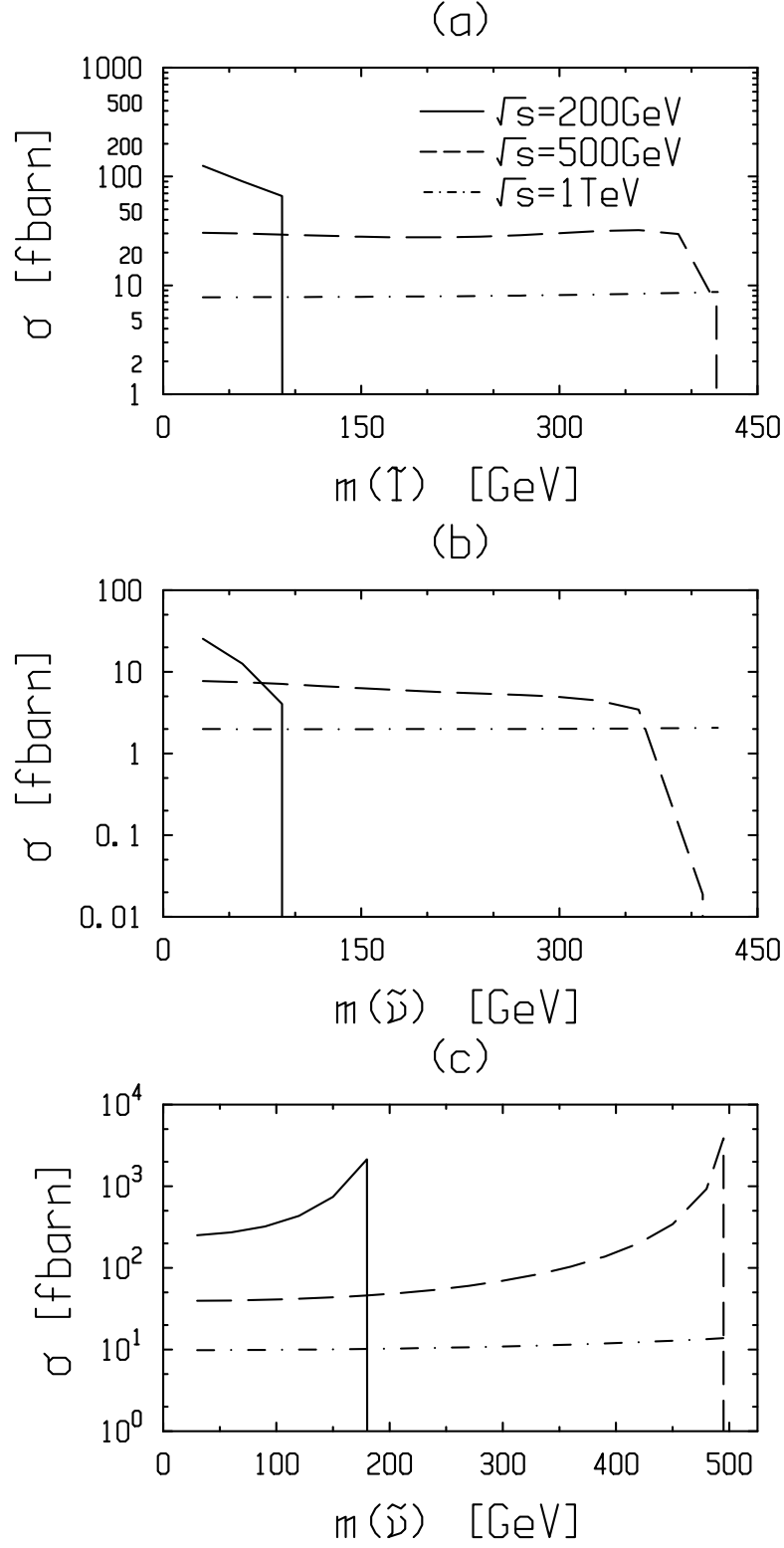


Figure 8: The cross sections for the processes,  $l_J^+ l_J^- \rightarrow \tilde{l}_m^- W^+$  (a),  $l_J^+ l_J^- \rightarrow \tilde{\nu}_m Z^0$  (b) and  $l_J^+ l_J^- \rightarrow \tilde{\nu}_m \gamma$  (c), are shown as a function of the slepton mass and the sneutrino mass, for  $\lambda_{mJJ} = 0.05$ . The three values of the center of mass energies considered are 200, 500 and 1000 GeV, as quoted in the top window.

#### 4.1.1 Inos production

The results for the integrated rates of the production of the lowest mass eigenstates  $\tilde{\chi}_1^-$  and  $\tilde{\chi}_1^0$ , at LEP II energies, are displayed in Figures 4 and 6, respectively. The inos production rates depend smoothly on  $\tan\beta$ , and on the mass parameters,  $\mu$ ,  $m_0$ ,  $M_2$ , in a way which closely reflects on the mass spectrum. Thus, the symmetry under  $\mu \leftrightarrow -\mu$  is upset only for low  $\tan\beta$  and the rates decrease with increasing  $M_2$ . The only cases where fast variations of rates arise are for values of  $m_0$  and  $M_2$  at which the center of mass energy hits on the sneutrino s-channel pole,  $\sqrt{s} = m_{\tilde{\nu}}$ . As  $m_0$  increases, the resonance occurs at smaller values of  $M_2$  since the sneutrino mass depends on  $M_2$ ,  $m_0$  and  $\tan\beta$  (see eq.(3)). The pole cross sections themselves, as parametrized by the conventional formula,

$$\begin{aligned}\sigma(l^+l^- \rightarrow X) &= \frac{8\pi s}{m_{\tilde{\nu}}^2} \frac{\Gamma(\tilde{\nu} \rightarrow l^+l^-)\Gamma(\tilde{\nu} \rightarrow X)}{(s - m_{\tilde{\nu}}^2)^2 + \Gamma_{\tilde{\nu}}^2} \\ &\approx 4 \cdot 10^8 \left(\frac{100\text{GeV}}{m_{\tilde{\nu}}}\right)^2 B(\tilde{\nu} \rightarrow l^+l^-) B(\tilde{\nu} \rightarrow X) \text{ fbarns},\end{aligned}\quad (5)$$

can grow to values several order of magnitudes higher. For clarity, we have refrained from drawing the cross sections close to the resonant energy in the same plot. This is the reason why the curves corresponding to  $M_2 = 150\text{GeV}$  do not appear in Figures 4(c)(d) and 6(c)(d). The effect of the pole can be seen for  $M_2 = 200\text{GeV}$  in Figures 4(a)(b) and 6(a)(b). We note also that for  $\mu = 0$ ,  $\tilde{\chi}_1^0$  is a pure higgsino and the  $\tilde{\chi}_1^0$  production cross section vanishes. The results for inos production rates at NLC or  $\mu^+\mu^-$  colliders center of mass energies are displayed in Figures 5 and 7. The drop with respect to the LEP II energies is nearly by one order of magnitude. The second neutralino production rates,  $\sigma(\tilde{\chi}_2^0) = \sigma(l_J^+l_J^- \rightarrow \tilde{\chi}_2^0\nu_m)$ , when this is kinematically allowed, turns out to be of the same order of magnitude as  $\sigma(\tilde{\chi}_1^0)$ . For  $\sqrt{s} = 500\text{GeV}$ ,  $\sigma(\tilde{\chi}_1^0)$  and  $\sigma(\tilde{\chi}_2^0)$  are numerically close throughout the parameter space of our model. However, for  $\sqrt{s} = 200\text{GeV}$ , there are regions (large  $\tan\beta$ ,  $\mu < 0$ ) where one has  $\sigma(\tilde{\chi}_2^0) \approx 2\sigma(\tilde{\chi}_1^0)$  and other regions (low  $\tan\beta$ ,  $\mu > 0$ ) where one rather has  $\sigma(\tilde{\chi}_2^0) \approx \frac{1}{2}\sigma(\tilde{\chi}_1^0)$ . As for the production rate of the second chargino,  $\sigma(\tilde{\chi}_2^-)$ , this is always nearly an order of magnitude below  $\sigma(\tilde{\chi}_1^-)$ .

#### 4.1.2 Sleptons production

The slepton and sneutrino production rates depend solely on the sleptons masses and  $\lambda_{mJJ}$ . The results, obtained by setting  $m_{\tilde{l}} = m_{\tilde{\nu}}$ , are displayed in Figure 8 for three values of the center of mass energies. An account of the mass difference between  $m_{\tilde{l}}$  and  $m_{\tilde{\nu}}$  would not change the numerical results in any significant way.

The differential cross section for the reaction  $l_J^+l_J^- \rightarrow \tilde{\nu}\gamma$  must be treated with special care because of its extreme sensitivity at the end points,  $x = \pm 1$ , in the limit of vanishing electron mass,  $m_e \rightarrow 0$ . As appears clearly on the expression of the squared momentum transfer variable,  $t = (k' - p')^2 = m_\gamma^2 - \frac{1}{2}(s - m_\nu^2 + m_\gamma^2)(1 - \frac{k}{E_k}\frac{p}{E_p}x)$ , for  $m_\gamma = 0$ , the t-channel amplitude has a collinear singularity,  $t \rightarrow 0$  as  $x \rightarrow 1$ . An analogous collinear singularity occurs for the u-channel amplitude,  $u = (k - p')^2 \rightarrow 0$  as  $x \rightarrow -1$ . Imposing the cut-off on the center of mass angle  $\theta$  makes the regularisation of collinear singularities pointless.

In the limit of vanishing  $m_\gamma$ , independently of  $x$  and  $m_e$ , the sneutrino production cross section becomes infinite at the limiting energy point,  $\sqrt{s} = m_{\tilde{\nu}}$ . This accounts for the property of the numerical results for the integrated cross section to rise with  $m_{\tilde{\nu}}$ , as seen in Figure 8(c). However, if one were to set  $m_\gamma$  at, say, the  $\rho$ -meson mass, in line with the vector meson dominance hypothesis, one would rather find the opposite behaviour with respect to the dependence on  $m_{\tilde{\nu}}$ . Observe that the increase of the cross section with  $m_{\tilde{\nu}}$  corresponds to the fact that, for  $m_{\tilde{\nu}} \approx \sqrt{s}$ , the process  $l_J^+l_J^- \rightarrow \tilde{\nu}\gamma$  behaves like a sneutrino resonant production, accompanied by the initial state radiation of a soft photon.

#### 4.1.3 Discussion

In summary, the single production rates range from several 10's of *fbarns* to a few 100's of *fbarns* at LEP energies and several units to a few 10's of *fbarns* at NLC energies. Therefore, the superpartners single production are at the limit of observability for LEP II assuming an integrated luminosity per year of  $200\text{pb}^{-1}$  at  $\sqrt{s} = 200\text{GeV}$ . The prospects for single production should be rather good at NLC [49] and  $\mu^+\mu^-$  colliders [50] since the assumed integrated luminosity per year is expected to be about  $50\text{fb}^{-1}$



at  $\sqrt{s} = 500\text{GeV}$ . Moreover, it is important to note here that had we considered for the RPV coupling constants, constant values for the product  $\lambda_{mJJ}(\frac{m_{\tilde{l}_R}}{100\text{GeV}})$ , rather than for  $\lambda_{mJJ}$ , the rates would get an important amplification factor  $(\frac{m_{\tilde{l}_R}}{100\text{GeV}})^2$  for increasing superpartners masses. Note that the slepton involved in the bound is of right chirality and thus is of opposite chirality than the slepton involved in the rate. Of course, the masses of  $\tilde{l}_L$  and  $\tilde{l}_R$  are related in a given model. At  $\sqrt{s} = 500\text{GeV}$  and assuming  $\lambda_{ijk} \geq 0.05$ , all the single production reactions should be potentially observable over a broad region of parameter space. The slepton production reactions could then probe slepton masses up to  $400\text{GeV}$  (Figure 8(a)) and sneutrino masses up to  $500\text{GeV}$  (Figure 8(c)). The ino production reactions could probe a large region of the parameter plane  $(\mu, M_2)$ , since the dependence on the parameters  $m_0$  and  $\tan\beta$  is smooth. To strengthen our conclusions, it is necessary to examine the signatures associated with the final states, which is the subject of the next section.

## 4.2 Branching Ratios

In the narrow resonance approximation, the partial transition rates are readily obtained by multiplying the total rates for each reaction with the decay branching fractions. The various final states for each of the  $2 \rightarrow 2$  single production reactions have been listed in Tables 1, 2 and 3. The leptons family configurations in the final states will depend on the hypothesis for the RPV coupling constant (single or pair dominance).

With the purpose of testing characteristic points of the parameter space, we have evaluated the branching ratios for the decays of the superpartners, namely,  $\tilde{\chi}_1^\pm, \tilde{l}^\pm$  and  $\tilde{\nu}$ , for variable  $\mu$  at discrete choices of  $M_2, m_0$  and  $\tan\beta$ , such that the main typical cases in the ordering of the masses  $m_{\tilde{\chi}_1^0}, m_{\tilde{\chi}_1^\pm}, m_{\tilde{l}}, m_{\tilde{\nu}}$ , can be explored. The results are shown in Figures 9, 10 and 11, for the chargino, the sneutrino and the slepton decays, respectively. The curves for the various branching ratios are distinguished by the same letters (numbers) as those used in Tables 1, 2 and 3 to label the various final states (decay processes). We shall now discuss in turn the various superpartner decay schemes corresponding to the five single production reactions.

### 4.2.1 Lowest mass Neutralino

The branching ratios for the  $\tilde{\chi}_1^0$  disintegrations are best analysed separately. For convenience, we do not treat the cases,  $m_{\tilde{\chi}_1^0} > m_{\tilde{q}}$  and  $m_{\tilde{\chi}_1^0} > m_{\tilde{\chi}_1^\pm}$ , since these arise marginally in most of the currently favored models (supergravity or gauge mediated soft supersymmetry breaking). The cascade decays which occur if  $m_{\tilde{\chi}_1^\pm} < m_{\tilde{\chi}_1^0}$  are also not considered since the corresponding region of the parameter space (Figure 3(c)) is forbidden by the experimental constraints on the inos masses. Thus, the process  $l_j^+ l_j^- \rightarrow \tilde{\chi}_1^0 \nu_m$  will only generate events with 2 leptons +  $\cancel{E}$ . At this point, it is necessary to specialize our discussion to a single dominant coupling constant hypothesis, assuming  $\lambda_{ijk} \neq 0$  not necessarily identical to  $\lambda_{mJJ}$ . One may distinguish the following four distinct cases. For an LSP  $\tilde{\chi}_1^0$ , namely,  $m_{\tilde{\chi}_1^0} < m_{\tilde{l}}, m_{\tilde{\nu}}$  (Case 1), only the direct RPV three-body decays,  $\tilde{\chi}_1^0 \rightarrow \bar{\nu}_i \bar{l}_j l_k$ ,  $\tilde{\chi}_1^0 \rightarrow \nu_i l_j \bar{l}_k$ , are allowed. The branching ratios are then determined on the basis of simple combinatoric arguments. For a dominant coupling constant, say,  $\lambda_{m11}$ , there are four final states:  $\nu_1 \bar{l}_m^- e^+$ ,  $\bar{\nu}_1 l_m^+ e^-$ ,  $\nu_m e^- e^+$  and  $\bar{\nu}_m e^+ e^-$ . Accordingly, the branching ratios of  $\tilde{\chi}_1^0$  into two charged leptons will depend on the type (flavor, charge) of the final state: The branching ratios equal  $\frac{1}{2}$  for the flavor diagonal  $e^+ e^-$  or flavor non diagonal  $l^\pm e^\mp$  channels,  $\frac{1}{4}$  for the fixed charges and flavors  $l^+ e^-$  or  $l^- e^+$  channels and 1 for the lepton-antilepton pairs of unspecified flavors. For a dominant coupling constant  $\lambda_{ijk} \neq \lambda_{m11}$ , an analogous result is obtained. For  $m_{\tilde{\chi}_1^0} > m_{\tilde{l}}, m_{\tilde{\nu}}$  (Case 2), the branching ratio for  $\tilde{\chi}_1^0$  decay is,

$$B(\tilde{\chi}_1^0 \rightarrow \bar{\nu}_i \bar{l}_j l_k) = \frac{\Gamma(\tilde{\chi}_1^0 \rightarrow \tilde{l}_j \bar{l}_j) B(\tilde{l}_j \rightarrow \bar{\nu}_i l_k) + \Gamma(\tilde{\chi}_1^0 \rightarrow \tilde{\nu}_i \bar{\nu}_i) B(\tilde{\nu}_i \rightarrow \bar{l}_j l_k)}{3\Gamma(\tilde{\chi}_1^0 \rightarrow \tilde{l}_j l_j) + 3\Gamma(\tilde{\chi}_1^0 \rightarrow \tilde{\nu}_i \nu_i)} = \frac{1}{3}, \quad (6)$$

where we have used the fact that in the present case, assuming a dominant coupling constant  $\lambda_{ijk}$ ,  $B(\tilde{l}_j \rightarrow \bar{\nu}_i l_k) = B(\tilde{\nu}_i \rightarrow \bar{l}_j l_k) = 1$ . The factors 3 in the denominator account for the number of families. For the intermediate case,  $m_{\tilde{\nu}} > m_{\tilde{\chi}_1^0} > m_{\tilde{l}}$  (Case 3), there occur contributions from 2-body RPC decays and 3-body RPV decays, such that:

$$B(\tilde{\chi}_1^0 \rightarrow \bar{\nu}_i \bar{l}_j l_k) = \frac{\Gamma(\tilde{\chi}_1^0 \rightarrow \bar{\nu}_i \bar{l}_j l_k) + \Gamma(\tilde{\chi}_1^0 \rightarrow \tilde{l}_j \bar{l}_j) B(\tilde{l}_j \rightarrow \bar{\nu}_i l_k)}{\Gamma(\tilde{\chi}_1^0 \rightarrow \bar{\nu}_i \bar{l}_j l_k) + 3\Gamma(\tilde{\chi}_1^0 \rightarrow \tilde{l}_j l_j)} \simeq \frac{1}{3}, \quad (7)$$

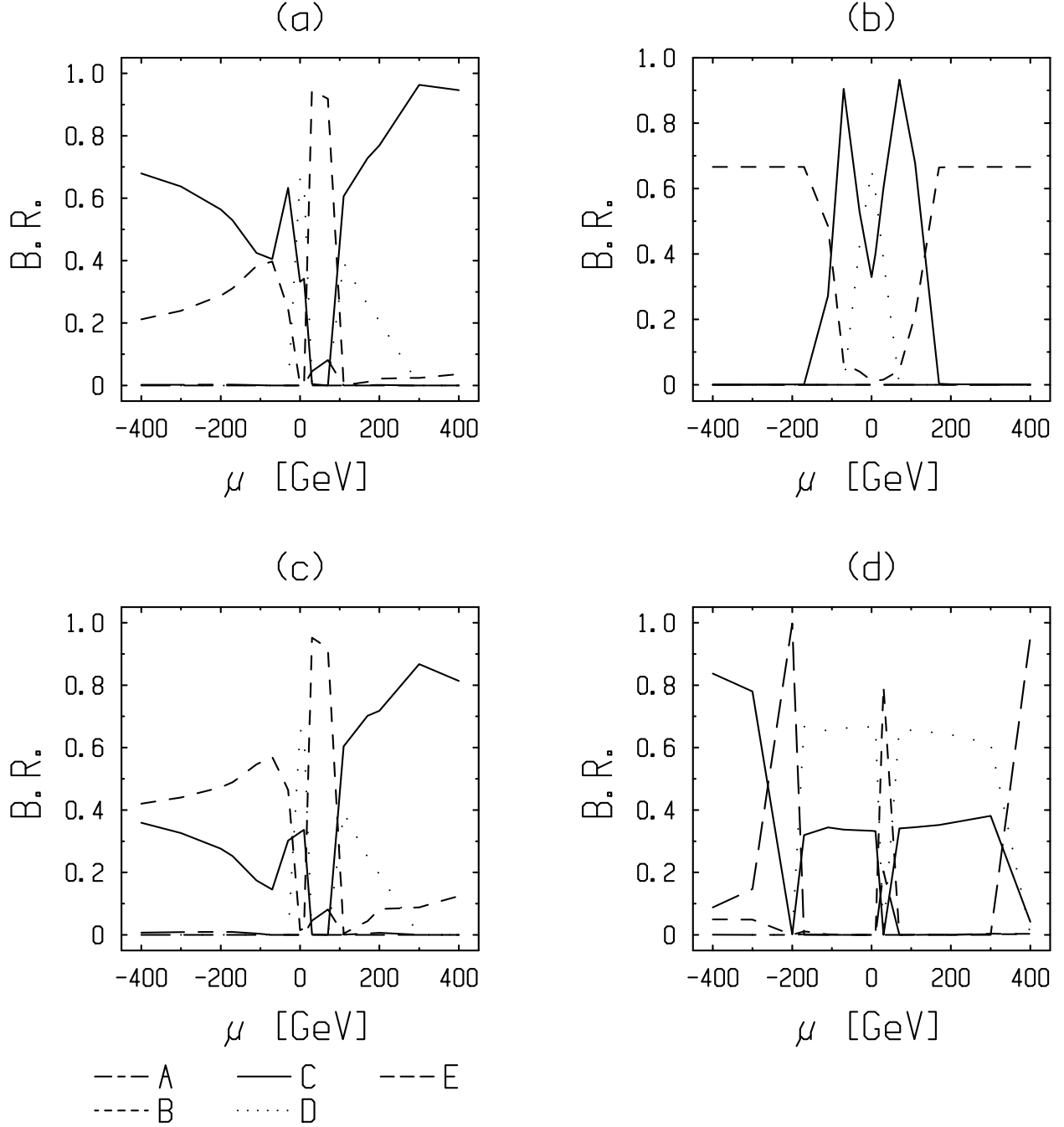


Figure 9: Branching ratios for the chargino  $\tilde{\chi}_1^-$  decays as a function of  $\mu$ . The results in the four windows are obtained with the following choices for the parameters,  $[(M_2(\text{GeV}), m_0(\text{GeV}), \tan \beta, \lambda_{ijk}), m_{\tilde{\nu}_L}(\text{GeV}), m_{\tilde{t}_L}(\text{GeV})]$ : (a)  $[(80, 20, 2, 0.05), 53.19, 81.66]$ , (b)  $[(80, 20, 50, 0.05), 34.20, 86.97]$ , (c)  $[(80, 20, 2, 0.1), 53.19, 81.66]$ , (d)  $[(200, 100, 2, 0.05), 195.6, 205.2]$ . The final states are labeled by the letters, A, B, C, D, E, which have the same meaning as in Table 1.

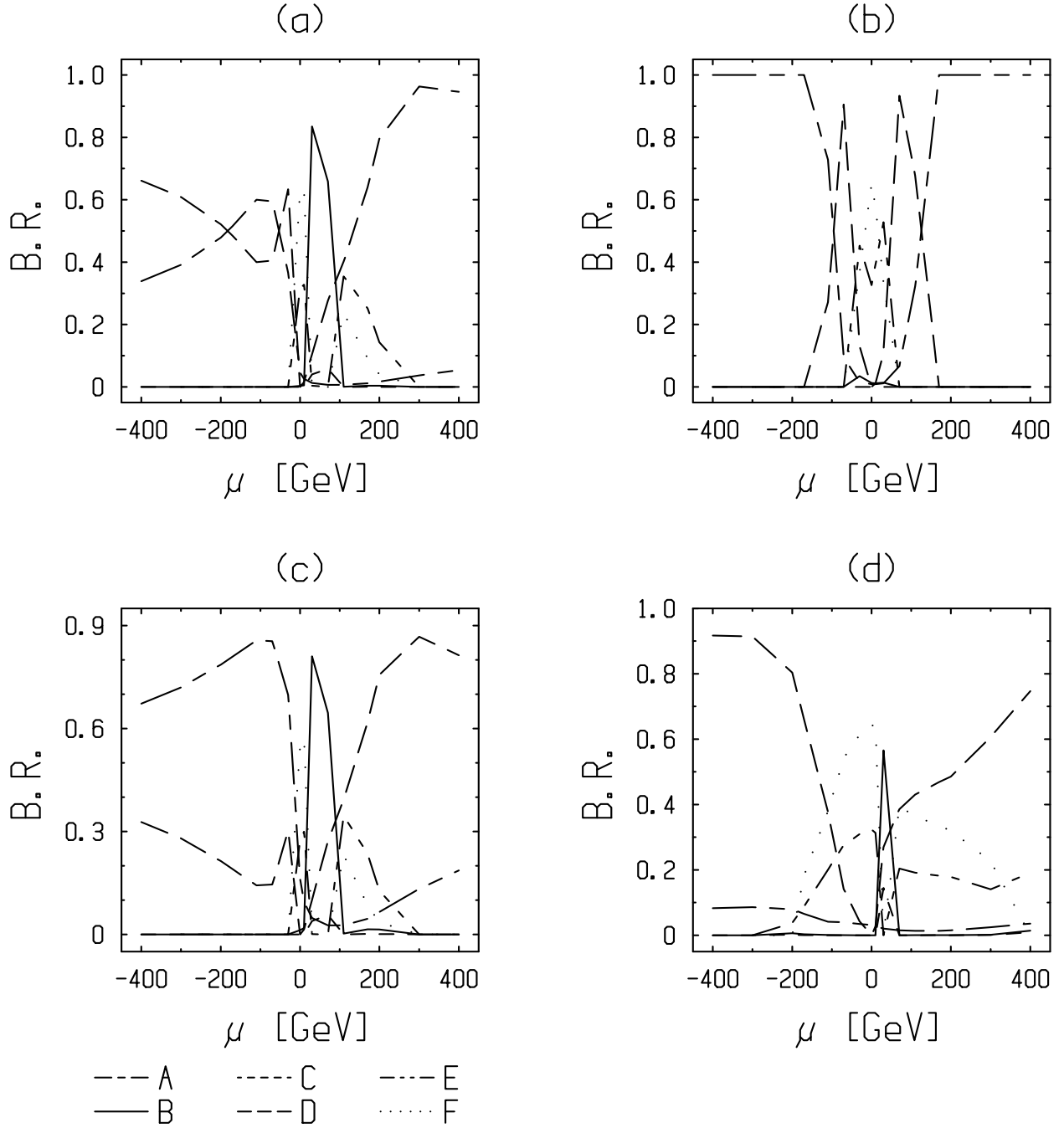


Figure 10: Branching ratios of the sneutrino decays as a function of  $\mu$ . The results in the four windows are obtained with the following choices for the parameters,  $[(M_2(\text{GeV}), m_0(\text{GeV}), \tan \beta, \lambda_{ijk}), m_{\tilde{\nu}_L}(\text{GeV}), m_{\tilde{t}_L}(\text{GeV})]$ : (a)  $[(80, 20, 2, 0.05), 53.19, 81.66]$ , (b)  $[(80, 20, 50, 0.05), 34.20, 86.97]$ , (c)  $[(80, 20, 2, 0.1), 53.19, 81.66]$ , (d)  $[(200, 100, 2, 0.05), 195.6, 205.2]$ . The final states are labeled by the letters, A, B, C, D, E, F, which have the same meaning as in Table 2.

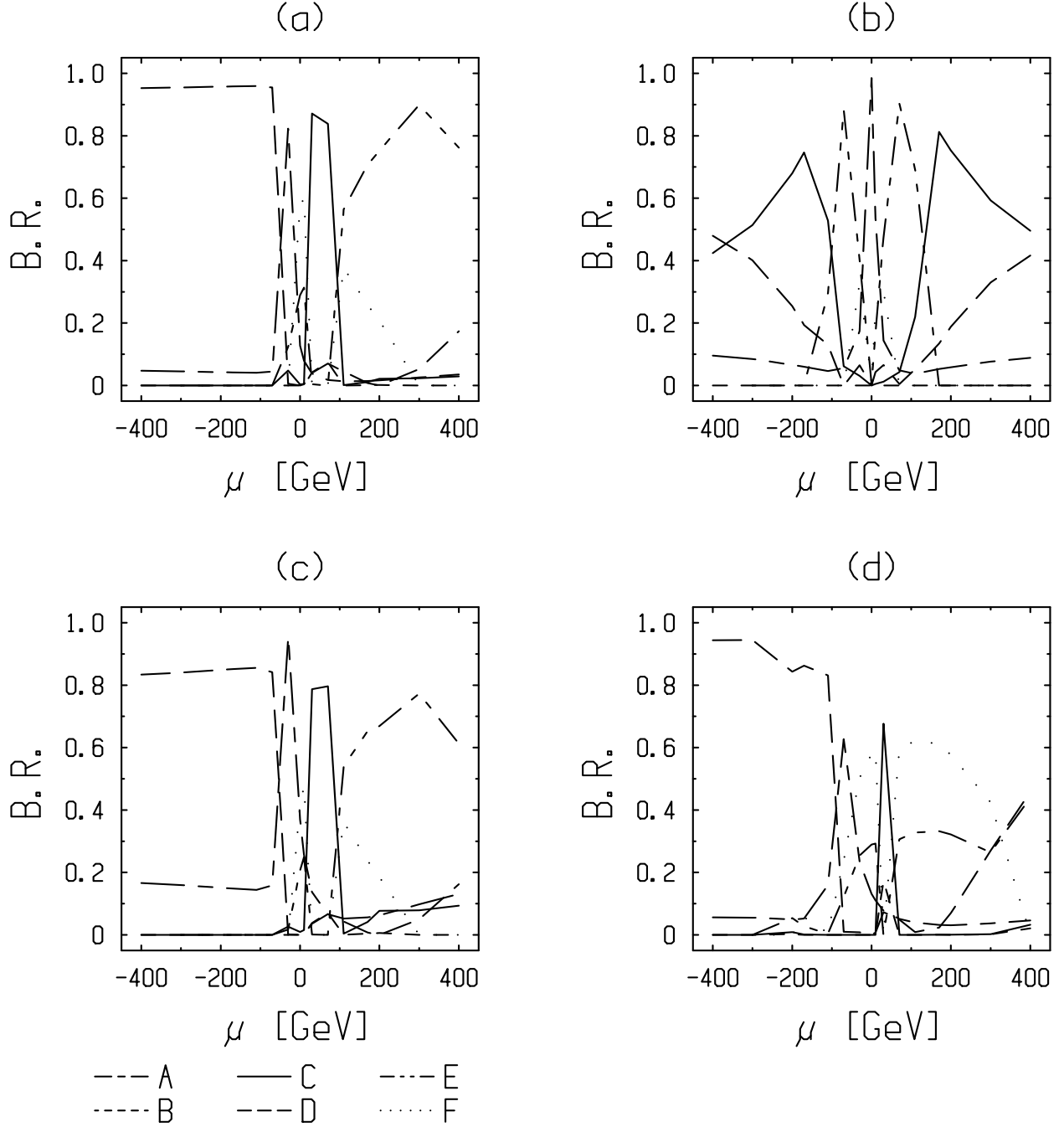


Figure 11: Branching ratios of the slepton decays as a function of  $\mu$ . The results in the four windows are obtained with the following choices for the parameters,  $[(M_2(\text{GeV}), m_0(\text{GeV}), \tan \beta, \lambda_{ijk}), m_{\tilde{\nu}_L}(\text{GeV}), m_{\tilde{t}_L}(\text{GeV})]$ : (a)  $[(80, 20, 2, 0.05), 53.19, 81.66]$ , (b)  $[(80, 20, 50, 0.05), 34.20, 86.97]$ , (c)  $[(80, 20, 2, 0.1), 53.19, 81.66]$ , (d)  $[(200, 100, 2, 0.05), 195.6, 205.2]$ . The final states are labeled by the letters, A, B, C, D, E, F, which have the same meaning as in Table 3.

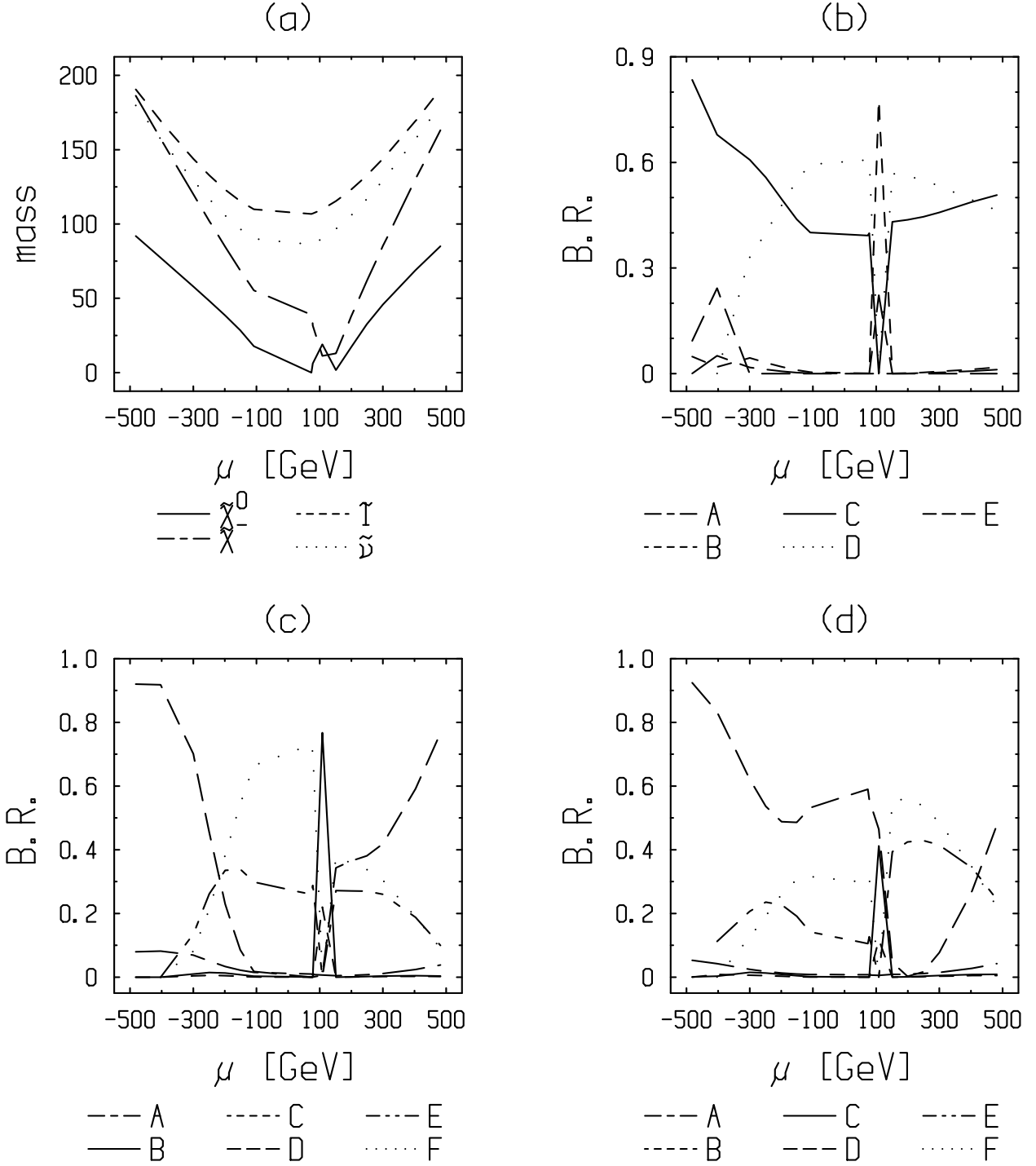


Figure 12: Mass spectrum of the supersymmetric particles (a), in GeV, and branching ratios for the decays of the chargino (b), sneutrino (c) and slepton (d), as a function of  $\mu$ . The results are obtained for  $m_0 = 100\text{GeV}$ , using equation (4). The final states in figures (b),(c),(d) are labeled by the letters, A,B,... which have the same meaning as in tables 1,2,3, respectively.

where the prime on  $\Gamma'$  is a reminder to indicate that the decay width includes only the contribution from a virtual sneutrino exchange. The approximate equality in eq.(7) derives from the fact that  $\Gamma'(\tilde{\chi}_1^0 \rightarrow \nu_i \tilde{l}_j l_k) \ll \Gamma(\tilde{\chi}_1^0 \rightarrow \tilde{l}_j \tilde{l}_j)$ , based on the expectation that an RPV 3-body decay should be much smaller than an RPC 2-body decay. An analogous argument to that of case 3 holds for the other intermediate case,  $m_{\tilde{l}} > m_{\tilde{\chi}_1^0} > m_{\tilde{\nu}}$  (Case 4). For the cases 2, 3 and 4, the multiplicity factors are the same as for the case 1. The  $\tilde{\chi}_1^0$  process may occur at the end stage in the decays of  $\tilde{\chi}_1^-$ ,  $\tilde{l}$  and  $\tilde{\nu}$ , to be discussed below. The associated  $\tilde{\chi}_1^0$  decay multiplicity factors for the two leptons final states will then take the same values as quoted above for the various selection criteria. In quoting numerical results below, we shall, for convenience, assume the case of unspecified lepton flavor and charge and thus will set the multiplicity factors to unity.

#### 4.2.2 Lowest mass Chargino

The results in Fig. 9 for the high  $\tan\beta$  case show a high degree of symmetry with respect to  $\mu \leftrightarrow -\mu$ , which arises from the symmetry in the inos mass spectrum (Figure 3(a)(b)). As can be seen from Figure 9(a), a dominant mode for the chargino at high values of  $|\mu|$  is the cascade decay,  $\tilde{\chi}^- \rightarrow \tilde{\chi}^0 l^- \tilde{\nu}$ , since this occurs via the two-body decay,  $\tilde{\chi}^- \rightarrow l^- \tilde{\nu}$  (C(7)). Indeed, for these high values of  $\mu$ , one has  $m_{\tilde{\nu}} < m_{\tilde{\chi}^-}$ . This two-body decay competes with the other two-body decay E,  $\tilde{\chi}^- \rightarrow \tilde{\chi}^0 W^-$ , when the latter is kinematically allowed, as is the case for  $\mu < -200 GeV$  in Figure 9(d). The difference between the values of the branching ratios C(7) and E is explained by the relative phase space factors of the associated rates. The RPV direct decays (A and B) are three-body decays with small coupling constant and are thus suppressed. In the case,  $m_{\tilde{\nu}} < m_{\tilde{\chi}^0} < m_{\tilde{\chi}^\pm}$ , the only open channel for the sneutrino is,  $\tilde{\nu} \rightarrow l \tilde{l}$ , so that the dominant mode for the chargino decay is the RPV decay B(4) (high values of  $|\mu|$  in Figure 9(b)). Even for  $m_{\tilde{\nu}} \approx m_{\tilde{\chi}^0}$ , the channel B(4) is competitive due to a small phase space ( $\mu \simeq -100 GeV$  in Figure 9(a)). In this case, for  $\lambda_{ijk} = 0.1$ , the direct RPV decay B(4) can become dominant (moderate negative values of  $\mu$  in Figure 9(c)). For small values of  $|\mu|$ , the difference between the two dominant leptonic (C) and hadronic (D) cascade decays is due to the flavor and color factors. We note also that in a small interval of  $\mu$  near  $\mu = 0$ ,  $m_{\tilde{\chi}_1^0} > m_{\tilde{\chi}_1^\pm}$  (see Figure 3), and consequently the only open channels are the direct RPV decays (Figure 9(a)(c)(d)). In this region, the direct RPV decay A(1) is negligible because the branching ratio depends on  $U_{11}$  which is small [51]. In conclusion, the highest branching ratios are associated with the cascade decays, C,D and E, except for the case in which the sneutrino is the LSP, where they are associated with the RPV decays B. The range of  $\mu$  for which the chargino  $\tilde{\chi}_1^-$  is the LSP is excluded by the experimental constraints on the inos masses (see Figure 3).

#### 4.2.3 Sneutrino

We turn now our attention to the sneutrino decays. For high values of  $\mu$ , the cascade decay D has the highest probability (Figure 10(a)(d)) since the decay into chargino is either kinematically forbidden or suppressed by a small phase space. As for the chargino study, the RPV direct decay A is of course small except when the competitive channel is reduced by a small phase space factor ( $\mu \approx -100 GeV$  in Figure 10(a)). In such a case, the RPV direct decay A may be important for values of  $\lambda_{ijk}$  near 0.1 (negative  $\mu$  in Figure 10(c)). When the sneutrino is the LSP, the RPV direct decay has a branching ratio equal to unity (Figure 10(b)). For small  $|\mu|$ , the decays E(6) and F(8) through charginos dominate the decay D through neutralinos. The reason is that for  $\mu = 0$ ,  $\tilde{\chi}_1^0$  is a pure higgsino, whose couplings are weak. In the so called higgsino limit,  $\mu \rightarrow 0$  [51], the decays B and C(3) are small since they occur through the  $\tilde{\chi}^-$  RPV direct decays. However, they have the highest probability if,  $m_{\tilde{\chi}_1^0} > m_{\tilde{\chi}_1^\pm}$  (Figure 10(a)(c)(d)). The relation between the leptonic (E) and hadronic (F) cascade decays can be explained in the light of the study on the chargino. We conclude that the cascade decays, B, D, E and F, are always the dominant modes, except when the sneutrino is the LSP.

#### 4.2.4 Slepton

Finally, we concentrate on slepton decays. For high values of  $\mu$ , the cascade decays via charginos are reduced because of a small phase space ( $|\mu| \approx 400 GeV$  in Figure 11(b) or for  $\mu < 0$  in Figures 11(c)(d)) or even closed (for  $\mu < 0$  in Figure 11(a)). In these cases, the decay D via neutralinos dominates. Elsewhere, the decays via charginos have higher branching ratios (for  $\mu > 0$  in Figures 11(a)(d)) since larger coupling

constants are involved. In the higgsino limit, the slepton cascade decay D via  $\tilde{\chi}_1^0$  is suppressed for the same reason as in the sneutrino study. The decay via  $\tilde{\chi}_1^-$  is then dominating. The interpretation of the difference between the decays, B, C, E and F, via charginos is based on the specific behaviours of the chargino branching ratios which have already been described above. We see in Figure 11(c), that for  $\lambda_{ijk} = 0.1$ , the RPV direct decay A is still very reduced. This is due to the important phase space for the slepton decay into neutralino. Lastly, a new phenomenon appears for the slepton case. In the higgsino limit ( $\mu \rightarrow 0$ ) at large  $\tan\beta$ , the matrix element  $U_{11} \rightarrow 0$  which forces the vertex  $\tilde{l} \tilde{\chi}^\pm \nu$  (see eq.B.3 in Appendix B) and the branching ratios for the cascade decays through the chargino to vanish [51]. This is the explanation of the fact that for  $\mu \simeq 0$ , one observes a peak of the direct RPV decay branching fraction (Figure 11(b)). Similar peaks are also observed at shifted  $\mu < 0$  for the low  $\tan\beta$  cases (Figures 11(a)(c)(d)). However this behaviour appears for ranges of the parameters which are forbidden by the bounds on the inos masses (Figure 3). The conclusion is that the cascade decays have always the highest probability for the reason that the L-chirality slepton cannot be the LSP in generic supergravity models.

#### 4.2.5 Discussion

In summary, we have learned that the general behaviour of branching ratios is mainly determined by the phase space and thus by the ordering of the supersymmetric particles masses. We have explored all the characteristic cases,  $m_{\tilde{\nu}} > m_{\tilde{\chi}_1^-} > m_{\tilde{\chi}_1^0}$ ,  $m_{\tilde{\chi}_1^-} > m_{\tilde{\nu}} > m_{\tilde{\chi}_1^0}$  and  $m_{\tilde{\chi}_1^-} > m_{\tilde{\chi}_1^0} > m_{\tilde{\nu}}$ . For high values of  $m_0$  lying above  $M_2$ , the sleptons would have masses greater than the inos masses. We have not analysed this case since one has then the same situation in the mass ordering as for the case of small values of  $|\mu|$  (except for large enough values of  $m_0$  where the on-shell  $W^\pm$  production can take place in  $\tilde{l}$  and  $\tilde{\nu}$  decays G). In this situation, as we have explained above, the charginos principally decay into neutralinos, while the sleptons and sneutrinos decay into charginos. The main conclusion is that the cascade decays are the dominant modes except if the sneutrino is the LSP. In this case, the RPV decay,  $\tilde{\chi}_1^- \rightarrow l_i \tilde{\nu}_i \rightarrow l_i l_j \tilde{l}_k$ , is dominant for the chargino decays, and the only open channel for the sneutrino is of course the direct RPV decay. Besides, for values of  $\lambda_{ijk}$  higher than 0.05, the RPV direct decay branching ratios can reach significant levels for the case where the cascade decays are suppressed due to small phase space factors.

The excitation of the second neutralino  $\tilde{\chi}_2^0$  deserves some attention since this may have in certain regions of the parameter space comparable, if not larger, production rates than the excitation of  $\tilde{\chi}_1^0$ . Assuming that the direct RPV widths are small enough so that the decay chain is initiated by the RPC contributions, then the desintegration mode,  $\tilde{\chi}_2^0 \rightarrow (\tilde{\chi}_1^0 + l^+ l^-)$ ,  $(\tilde{\chi}_1^0 + \bar{\nu} \nu)$ , will also yield  $2l + \cancel{E}$  and  $4l + \cancel{E}$  final states, respectively, and the other desintegration modes,  $\tilde{\chi}_2^0 \rightarrow (\tilde{\chi}_1^+ + l^- \bar{\nu}, \tilde{\chi}_1^- + l^+ \nu)$ ,  $(\tilde{\nu} \nu, \tilde{\nu} \bar{\nu})$ ,  $(\tilde{l}^\pm l^\mp)$ , will yield  $2l + \cancel{E}$  and  $4l + \cancel{E}$  final states according to decay schemes similar to those given in Tables 2,3,1. In our supergravity models, the  $\tilde{\chi}_2^0$  decay into  $\tilde{\chi}_1^\pm$  should be suppressed by a small phase space (Fig.3). To determine which of the decay modes,  $\tilde{\chi}_2^0 \rightarrow \tilde{\chi}_1^0$ ,  $\tilde{l}$  or  $\tilde{\nu}$ , leads to the dominant signal would require a detailed comparison of branching ratios at the initial as well as the subsequent stages.

Let us ask in what way would alternate hypotheses on the family dependence affect our conclusions. Especially regarding the multiplicities of final states, this is relevant for the cases,  $m_{\tilde{\chi}_1^-} > m_{\tilde{l}}, m_{\tilde{\nu}}$ , where the chargino can cascade decay to on-shell sleptons or sneutrinos (A(2) and B(4) in Table 1). As we have emphasized in the last paragraph of Section 2.2, the chargino decays have a multiplicity of 2 for three degenerate families of sleptons. For the case of two degenerate families, labeled by the indices,  $m, n$ , assuming a dominant RPV coupling constant  $\lambda_{ijk}$ , the multiplicity equals 2 for  $(m, n) = (i, j)$ , since the two sleptons from families  $i$  and  $j$  can be produced on-shell, and equals 1 for  $m = k$  or  $n = k$ . For the physically interesting case of a single low mass family, labeled by the index,  $m$ , one finds that the multiplicity equals 1 for  $m \neq k$  and 0 otherwise. The conclusion is that the RPV contributions A and B (in Table 1) to the chargino branching ratios increase as the number of slepton families, which are lower in mass than the chargino, becomes higher. This effect, which is quite small, would affect the branching ratios in parameters regions for which the RPV contributions A and B are not weak, that is for  $\mu < 0$  in Figures 9(a)(b)(c).

In Figure 12, we present results for the branching fractions for fixed  $m_0$  in the infrared fixed point model with electroweak symmetry breaking. In this constrained version, where  $m_{1/2}$  varies with  $\mu$ , the dependence on  $\mu$  is rather similar to that of the non minimal model where we worked instead with fixed  $m_0$  and  $m_{1/2}$ . However, as we see from the mass spectrum, here the LSP is the neutralino  $\tilde{\chi}_1^0$  for all the physical ranges of the parameters. Due to the large mass difference between the  $\tilde{\chi}_1^0$  LSP and the NLSP (next to LSP), the cascade decays are the only dominant modes and the branching ratios for the RPV

direct decays are very weak.

Let us add a few qualitative remarks on the predictions of gauge mediated supersymmetry breaking models. In order for the production rates in the minimal model [52] to have the same order of magnitude as those obtained in the supergravity model of section 4, one needs a parameter  $\Lambda = \frac{F}{M} \simeq 10^4 GeV$ , using familiar notations for the supersymmetry breaking scale ( $\sqrt{F}$ ) and messenger scale ( $M$ ). Concerning the signals, by comparing the mean free paths for  $\tilde{\chi}_1^0$  (favourite candidate for LSP) in both models, one finds that the decay channel to the gravitino,  $\tilde{\chi}_1^0 \rightarrow \gamma \tilde{G}$ , becomes competitive with the RPV decay channel,  $\tilde{\chi}_1^0 \rightarrow \nu \bar{l}$ , for,  $\frac{\sqrt{\langle F \rangle}}{100 TeV} \leq \frac{10^{-2}}{\sqrt{\Lambda}}$ .

Let us also comment briefly on some of the experimental issues. A given final state can possibly arise simultaneously from several of the single production processes. The important  $4l + \cancel{E}$  signal which occurs for  $\tilde{\chi}^\pm, \tilde{l}^\pm, \tilde{\nu}$  productions is one such example where one may be forced to add all three types of cross sections in comparing with some given experimental data sample. Similarly, for most signals, one must typically add the contributions from the two charge conjugate partner processes. Concerning the competition with the standard model background, one expects that the most important contributions to the final states,  $2l + \cancel{E}$  and  $4l$ , will arise from the reactions,  $l_J^+ l_J^- \rightarrow W^+ l^- \bar{\nu}, W^- l^+ \nu, W^+ W^-, Z^0 l^+ l^-, Z^0 Z^0, Z^0 \gamma$ . In spite of the large standard model rates of order one picobarn at  $\sqrt{s} = 500 GeV$  [38], one should be able to distinguish the single production signals by exploiting their specific non diagonal flavor character (final state B in Table 3 and A in Table 2). The other multileptons final states, generated by the cascade decays,  $4l + \cancel{E}, 4l + Z^0, 3l + Z^0 + W^\pm + \cancel{E}, \dots$  have a standard model background which is negligible. The potentially large two photons background processes, induced by  $\gamma\gamma$  photons pairs radiated by the initial leptons, can be significantly reduced by imposing suitable cuts on the leptons transverse momenta. Finally, we note that the selection by the RPV single production of identical helicities for the initial state,  $l_H^+ l_H^+$ , can be exploited to discriminate against the minimal supersymmetric standard model and also the standard model, for which the identical helicities configuration only appears with the t-channel Z-boson exchange.

## 5 Dynamical distributions

The distributions of rates with respect to kinematical variables associated with the final states offer helpful means to characterize the underlying production processes. As an indicative study we shall present here some characteristic dynamical distributions obtained for the production reactions,  $l_J^+ l_J^- \rightarrow \tilde{\chi}_1^\pm l^\mp, \tilde{\chi}_1^0 \nu, \tilde{\chi}_1^0 \bar{\nu}, \tilde{\chi}_2^0 \nu, \tilde{\chi}_2^0 \bar{\nu}$ , from a Monte Carlo events simulation for which we have used the event generator SUSYGEN [41]. We concentrate on the final state signals of  $2l + \cancel{E}$ ,  $4l$  and  $4l + \cancel{E}$ . Note that for high values of  $\mu$ , the final state  $4l + \cancel{E}$  is the dominant mode for the chargino, slepton and sneutrino decays. This signal also receives contributions from the reactions,  $l_J^+ l_J^- \rightarrow \tilde{\nu} Z^0 (\tilde{\nu} Z^0), \tilde{\nu} \gamma (\tilde{\nu} \gamma), \tilde{l}^\pm W^\mp$ , which however are not included in the simulation. The standard model background is expected to be small for the  $4l + \cancel{E}$  signal. The main background from the minimal supersymmetric standard model interactions arises from the neutralino RPC pair production,  $l_J^+ l_J^- \rightarrow \tilde{\chi}_1^0 \tilde{\chi}_1^0$ . Following the analysis in [53], we consider an incident energy of  $\sqrt{s} = 350 GeV$  and use a non minimal supergravity model for which we choose the set of parameters,  $M_2 = 250 GeV, \mu = 400 GeV, m_0 = 70 GeV, \tan \beta = 2$ , which yields the spectrum,  $m_{\tilde{\chi}_1^0} = 118.5 GeV, m_{\tilde{\chi}_2^0} = 221.4 GeV, m_{\tilde{\chi}_1^\pm} = 219.1 GeV, m_{\tilde{\nu}_L} = 225 GeV, m_{\tilde{l}_L} = 233 GeV, m_{\tilde{l}_R} = 141 GeV$ . The integrated rates (ignoring acceptance cuts) are, for  $\lambda_{mJJ} = 0.05$  [ $m = 2$ ],  $\sigma(\tilde{\chi}_1^+ \mu^-) = 30.9 fb, \sigma(\tilde{\chi}_1^0 \nu_\mu) = 4.8 fb, \sigma(\tilde{\chi}_2^0 \nu_\mu) = 12.1 fb$  and  $\sigma(\tilde{\chi}_1^0 \tilde{\chi}_1^0) = 238.9 fb$ . We consider the following five dynamical variables for all types of final states: Invariant missing energy,  $E_m = \sum_{i \in \nu} E_i$  where the sum is over the neutrinos, as appropriate to a broken R parity situation; Average per event of the  $\mu^\pm$  lepton transverse momentum,  $P_t(\mu^\pm) = \frac{\sum_i |p_t(\mu_i^\pm)|}{N_\mu}$ , where  $N_\mu$  is the number of muons; Angle between the momenta of same electric charge sign (SS) muons pairs; Average per event of the summed transverse momenta for leptons pairs of same sign (SS) or opposite sign (OS),  $P_t^{SS,OS}(ll) = \sum_{(i,j)} \frac{p_t(l_i^{\pm,\mp}) + p_t(l_j^{\pm,\mp})}{N}$ , where  $N$  is the number of configurations and  $l = e, \mu$ .

We have generated the inos single production and the  $\tilde{\chi}_1^0$  pair production in separate samples of 5000 events each. Our choice of using equal number of events for both reactions has been made on the basis of the following three somewhat qualitative considerations, none of which is compelling. First, the single production reactions occur in company of their charge conjugate partners, which multiplies rates by a factor 2. Second, the other  $\tilde{\nu}$  and  $\tilde{l}$  single production reactions, which have not been included, would be expected to add contributions of similar size to the leptonic distributions. Third, assuming for the RPV



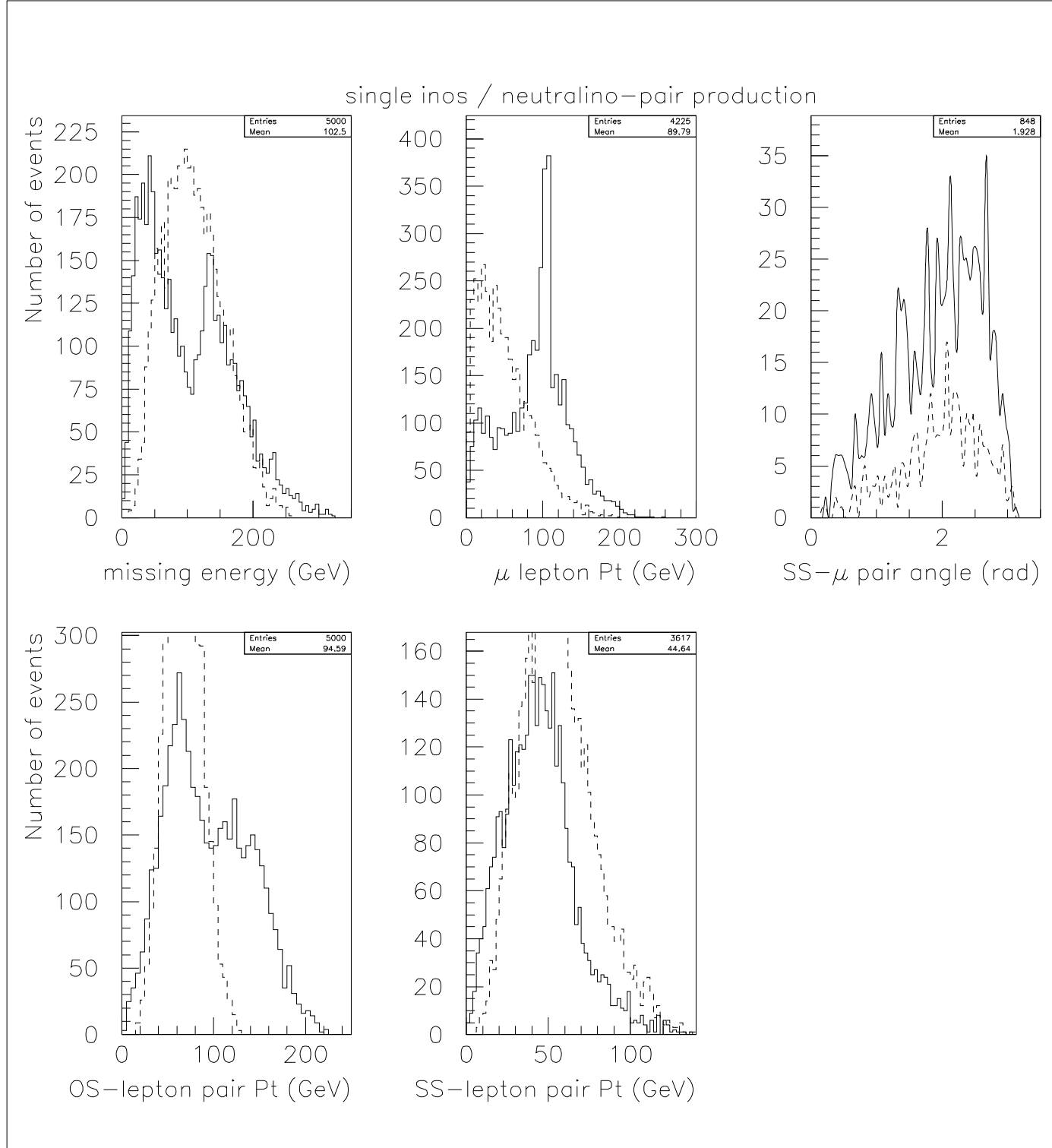


Figure 13: Distributions of missing energy, muon transverse momentum, same sign muon pair angle, summed transverse momentum for opposite sign (OS) and same sign (SS) leptons pairs (electrons and muons) for the single production processes,  $l_J^+ l_J^- \rightarrow \tilde{\chi}_1^\pm \mu^\mp, \tilde{\chi}_1^0 \nu_\mu, \tilde{\chi}_1^0 \bar{\nu}_\mu, \tilde{\chi}_2^0 \nu_\mu, \tilde{\chi}_2^0 \bar{\nu}_\mu$  (solid line), and the pair production process,  $l_J^+ l_J^- \rightarrow \tilde{\chi}_1^0 \tilde{\chi}_1^0$  (dashed line), at a center of mass energy of 350 GeV. The parameters values are,  $M_2 = 250 \text{ GeV}$ ,  $m_0 = 70 \text{ GeV}$ ,  $\mu = 400 \text{ GeV}$ ,  $\tan \beta = 2$ ,  $\lambda_{211} = 0.05$ . Events samples, consisting of 5000 events each, are generated for the inos single production and neutralino pair production, respectively.

coupling constant the alternative bound,  $\lambda_{mJJ} \frac{100\text{GeV}}{m_{\tilde{l}_R}} < 0.05$ , there would result a relative enhancement for single production over pair production by a factor,  $(\frac{m_{\tilde{l}_R}}{100\text{GeV}})^2$ . The above three points motivate our rough guess that the number of events chosen for the five single production processes (together with their charge conjugate partners) should be of comparable size to that of the  $\tilde{\chi}_1^0$  pair production process.

The results are shown in Figure 13. The single production reactions present certain clear characteristic features: Concentration of missing energy  $E_m$  at low energies; pronounced peaks in the muon transverse momentum  $P_t(\mu^\pm)$  and in the angular distribution for the same sign muons pairs; and a double peak in the transverse momentum distribution for the opposite sign leptons pairs,  $P_t^{OS}(\ell\ell)$ . The large transverse momentum components present in the single production distributions in  $P_t^{OS}(\ell\ell)$  and in  $P_t(\mu^\pm)$  are explained by the fact that one of the two leptons (namely,  $l_m^\pm$ ) is created at the production stage. Similarly, the existence of a strong angular correlation between same sign muons pairs is interpreted naturally by the momentum conservation balance between the lepton  $l_m^\pm$  produced in the initial stage and the other lepton produced at the decay stage. Although there are certain distinguishing properties between the single and pair production processes, the discrimination between the two may depend crucially on the relative sizes of the associated event samples. Of course, the best possible situation would be for an energetically forbidden neutralino pair production.

Finally, we comment on the effect of eventually excluding the  $\tilde{\chi}_2^0$  single production component. In that case, most of the signals for single production would become less diluted in comparison with neutralino pair production, the large missing energy signal would be removed while the large OS lepton pair  $P_t^{OS}(\ell\ell)$  signal would become amplified.

## 6 Conclusions

We have analysed the full set of  $2 \rightarrow 2$  single production processes at leptonic colliders induced by the RPV interactions  $LLE^c$ , within a supergravity model. Although our approximate study has obvious limitations (factorisation and narrow resonance approximation, neglect of the spin correlations and omission of acceptance cuts), it uncovers the general trends of all the 5 single production reactions. Over the whole parameter space, for an RPV coupling constant  $\lambda_{mJJ}$  of order 0.05, the integrated rates are of comparable order of magnitudes although  $\tilde{\chi}_1^\pm$  and  $\tilde{\nu}$  are typically larger by factors of 2 compared to  $\tilde{l}$  production and by factors of 5 compared to  $\tilde{\chi}_1^0$  production. The detectability for each single production separately is modest at LEP II but comfortable at NLC, corresponding to a few events and a few thousands of events per year, respectively. A wide region of the parameter space can be probed at  $\lambda_{mJJ} > 0.05$ . In spite of the rich variety of final states, the dominant signals arise from the single or double RPC induced cascade decays to the LSP, which are also favored by phase space arguments. For the minimal supergravity model, assuming electroweak symmetry breaking, large mass differences occur between the scalar superpartners and the  $\tilde{\chi}_1^0$  LSP, leading to dominant cascade decays modes with weak competitiveness from the RPV direct decays. The signals,  $4l + \cancel{E}, 6l, 6l + \cancel{E}$ , arising from cascade decays are free from standard model background which make them quite interesting signatures for the discovery of supersymmetry and R parity violation. Even the  $4l$  signal arising from direct RPV decays could be observable due to a characteristic non diagonal flavor configuration. For center of mass energies well above all the thresholds, the  $4l + \cancel{E}$  signal receives contributions from all five single production processes and hence should be strongly amplified. We have presented some dynamical distributions for the final states which could characterise the single production reactions.

## 7 Acknowledgments

We are grateful to R. Barbier and S. Katsanevas for guidance in using the events generator SUSYGEN, to P. Lutz and the Direction of the DAPNIA at Saclay for providing us, through the DELPHI Collaboration, an access to the ANASTASIE computer network at Lyon and to P. Micout for his technical help on that matter. We thank M. Besançon, F. Ledroit, R. Lopez and G. Sajot for helpful discussions.

## A Formulas for spin summed amplitudes

We discuss the five  $2 \rightarrow 2$  body single production processes given by eq.(1). The formulas for the probability amplitudes are:

$$\begin{aligned}
M(\tilde{\chi}_a^- + l_m^+) &= \frac{g\lambda_{mJJ}V_{a1}^*}{s - m_{\tilde{\nu}_{mL}}^2} \bar{v}(k') P_L u(k) \bar{u}^c(p) P_L v(p') - \frac{g\lambda_{mJJ}V_{a1}^*}{t - m_{\tilde{\nu}_{JL}}^2} \bar{u}^c(p) P_L u(k) \bar{v}(k') P_L v(p'), \\
M(\tilde{\chi}_a^0 + \tilde{\nu}_m) &= + \frac{\sqrt{2}g\lambda_{mJJ}}{s - m_{\tilde{\nu}_{mL}}^2} \frac{1}{2} (N_{a2}^* - tg\theta_W N_{a1}^*) \bar{u}(p) P_L v(p') \bar{v}(k') P_L u(k) \\
&\quad + \frac{\sqrt{2}g\lambda_{mJJ}}{t - m_{\tilde{l}_{JL}}^2} \frac{1}{2} (N_{a2}^* + tg\theta_W N_{a1}^*) \bar{u}(p) P_L u(k) \bar{v}(k') P_L v(p') \\
&\quad + \frac{\sqrt{2}g\lambda_{mJJ}}{u - m_{\tilde{l}_{JR}}^2} (tg\theta_W N_{a2}^*) \bar{v}^c(p') P_L u(k) \bar{v}(k') P_L v(p), \\
M(\tilde{l}_{mL}^-(p) + W^+(p')) &= \frac{g\lambda_{mJJ}^*}{\sqrt{2}(s - m_{\tilde{\nu}_{mL}}^2)} 2p \cdot \epsilon(p') \bar{v}(k') P_R u(k) + \frac{g\lambda_{mJJ}^*}{\sqrt{2}t} \bar{v}(k') \gamma \cdot \epsilon(p') (\not{p} - \not{k}) P_R u(k), \\
M(\tilde{\nu}_{mL}(p) + Z(p')) &= \frac{g\lambda_{mJJ}^*}{2\cos\theta_W} \left[ \frac{\bar{v}(k') \gamma \cdot \epsilon(p') (\not{k} - \not{p}) a_L(e) P_R u(k)}{t - m_{\tilde{l}_J}^2} \right. \\
&\quad \left. + \frac{\bar{v}(k') a_R(e) P_R (\not{k} - \not{p}') \gamma \cdot \epsilon(p') u(k)}{u - m_{\tilde{l}_J}^2} + \frac{\bar{v}(k') a_L(\tilde{\nu}) P_R u(k) 2p \cdot \epsilon(p')}{s - m_{\tilde{\nu}_{mL}}^2} \right], \\
M(\tilde{\nu}_{mL}(p) + \gamma(p')) &= -e\lambda_{mJJ}^* \left[ \frac{\bar{v}(k') \gamma \cdot \epsilon(p') (\not{k} - \not{p}) P_R u(k)}{t - m_{\tilde{l}_J}^2} + \frac{\bar{v}(k') (\not{k} - \not{p}') \gamma \cdot \epsilon(p') P_R u(k)}{u - m_{\tilde{l}_J}^2} \right]. \quad (A.1)
\end{aligned}$$

In deriving the results for the inos production amplitudes, we have systematically neglected their higgsino components. The parameters in the  $Z^0 f \bar{f}$  and  $Z^0 \tilde{f} \tilde{f}$  vertices denoted as,  $a_H(f) = a(f_H)$  and  $a_H(\tilde{f}) = a(\tilde{f}_H)$ , are defined by,  $a(f_H) = a(\tilde{f}_H) = 2T_3^H(f) - 2Qx_W$ , with  $H = [L, R]$  and  $x_W = \sin^2 \theta_W$ . Throughout this work, our notations follow closely the Haber-Kane conventions [48].

The unpolarized cross sections in the center of mass frame are given by the familiar formula,  $d\sigma/d\cos\theta = p/(128\pi ks) \sum_{pol} |M|^2$ , where the sums over polarizations for the probability amplitudes squared are given by:

$$\begin{aligned}
\sum_{pol} |M(\tilde{\chi}_a^- + l_m^+)|^2 &= |\lambda_{mJJ} g V_{a1}^*|^2 \left[ \frac{s(s - m_{\tilde{\chi}_a^-}^2 - m_{l_m}^2)}{|R_s(\tilde{\nu}_{mL})|^2} + \frac{(m_{\tilde{\chi}_a^-}^2 - t)(m_{l_m}^2 - t)}{|R_t(\tilde{\nu}_{JL})|^2} \right. \\
&\quad \left. - \operatorname{Re} \left( \frac{(s(s - m_{\tilde{\chi}_a^-}^2 - m_{l_m}^2) + (m_{\tilde{\chi}_a^-}^2 - t)(m_{l_m}^2 - t) - (m_{\tilde{\chi}_a^-}^2 - u)(m_{l_m}^2 - u))}{R_s(\tilde{\nu}_{mL}) R_t^*(\tilde{\nu}_{JL})} \right) \right], \quad (A.2)
\end{aligned}$$

$$\begin{aligned}
\sum_{pol} |M(\tilde{\chi}_a^0 + \tilde{\nu}_m)|^2 &= \frac{g^2}{2} |\lambda_{mJJ}|^2 \left[ |N_{a2} + tg\theta_W N_{a1}|^2 \frac{t(t - m_{\tilde{\chi}_a^0}^2)}{|R_t(\tilde{l}_{JL})|^2} \right. \\
&\quad + 4|tg\theta_W N_{a2}|^2 \frac{u(u - m_{\tilde{\chi}_a^0}^2)}{|R_u(\tilde{l}_{JR})|^2} + |N_{a2} - tg\theta_W N_{a1}|^2 \frac{s(s - m_{\tilde{\chi}_a^0}^2)}{|R_s(\tilde{\nu}_{mL})|^2} \\
&\quad - \operatorname{Re} \left( (N_{a2}^* - tg\theta_W N_{a1}^*) (-N_{a2} - tg\theta_W N_{a1}) \frac{(s(s - m_{\tilde{\chi}_a^0}^2) - t(m_{\tilde{\chi}_a^0}^2 - t) + u(m_{\tilde{\chi}_a^0}^2 - u))}{R_s(\tilde{\nu}_{mL}) R_t^*(\tilde{l}_{JL})} \right. \\
&\quad + 2(N_{a2}^* - tg\theta_W N_{a1}^*) (-tg\theta_W N_{a2}) \frac{(s(s - m_{\tilde{\chi}_a^0}^2) - u(m_{\tilde{\chi}_a^0}^2 - u) + t(m_{\tilde{\chi}_a^0}^2 - t))}{R_s(\tilde{\nu}_{mL}) R_u^*(\tilde{l}_{JR})} \\
&\quad \left. \left. + 2(-N_{a2}^* - tg\theta_W N_{a1}^*) (-tg\theta_W N_{a2}) \frac{(-u(m_{\tilde{\chi}_a^0}^2 - u) - t(m_{\tilde{\chi}_a^0}^2 - t) - s(s - m_{\tilde{\chi}_a^0}^2))}{R_t(\tilde{l}_{JL}) R_u^*(\tilde{l}_{JR})} \right) \right], \quad (A.3)
\end{aligned}$$

$$\sum_{pol} |M(\tilde{l}_{mL}^- + W^+)|^2 = \frac{sg^2 |\lambda_{mJJ}|^2}{2|R_s(\tilde{\nu}_{mL})|^2} \left( \frac{(s - m_{\tilde{l}_{mL}}^2 - m_W^2)^2}{m_W^2} - 4m_{\tilde{l}_{mL}}^2 \right) - \frac{g^2 |\lambda_{mJJ}|^2}{2|t|^2}$$

$$\begin{aligned}
& \times \left[ (m_{\tilde{l}_{mL}}^2 - t)(m_W^2 - t) + st + \frac{m_W^2 - t}{m_W^2} \left( (m_{\tilde{l}_{mL}}^2 - t)(m_W^2 + t) + t(m_W^2 - u) \right) \right] \\
& - g^2 Re \frac{\lambda_{mJJ} \lambda_{mJJ}^*}{t R_s^*(\tilde{\nu}_{mL})} [(m_{\tilde{l}_{mL}}^2 - t)(m_{\tilde{l}_{mL}}^2 - u) + s(m_{\tilde{l}_{mL}}^2 - u) + (m_{\tilde{l}_{mL}}^2 - t)(m_W^2 - t) \\
& - \frac{s(s - m_W^2 - m_{\tilde{l}_{mL}}^2)(m_W^2 - t)}{m_W^2}], \tag{A.4}
\end{aligned}$$

$$\begin{aligned}
\sum_{pol} |M(\tilde{\nu}_{mL} + Z)|^2 &= \frac{g^2 |\lambda_{mJJ}|^2}{\cos^2 \theta_W} Re \left[ \frac{s}{|R_s(\tilde{\nu}_{mL})|^2} \left( \frac{(s - m_{\tilde{\nu}_{mL}}^2 - m_Z^2)^2}{4m_Z^2} - m_{\tilde{\nu}_{mL}}^2 \right) \right. \\
& - \frac{(\sin^2 \theta_W)^2}{|R_u(l_J)|^2} \left( (m_{\tilde{\nu}_{mL}}^2 - u)(m_Z^2 - u) + su + \frac{m_Z^2 - u}{m_Z^2} ((m_{\tilde{\nu}_{mL}}^2 - u)(m_Z^2 + t) + u(m_Z^2 - t)) \right) \\
& - \frac{(2 \sin^2 \theta_W - 1)^2}{4|R_t(l_J)|^2} \left( (m_{\tilde{\nu}_{mL}}^2 - t)(m_Z^2 - t) + st + \frac{m_Z^2 - t}{m_Z^2} ((m_{\tilde{\nu}_{mL}}^2 - t)(m_Z^2 + t) + t(m_Z^2 - u)) \right) \\
& - \frac{(\sin^2 \theta_W)}{R_u(l_J) R_s^*(\tilde{\nu}_{mL})} \left( (m_{\tilde{\nu}_{mL}}^2 - t)(m_{\tilde{\nu}_{mL}}^2 - u) + s(m_{\tilde{\nu}_{mL}}^2 - t) + (m_{\tilde{\nu}_{mL}}^2 - u)(m_Z^2 - u) \right) \\
& - \frac{s}{m_Z^2} (s - m_{\tilde{\nu}_{mL}}^2 - m_Z^2)(m_Z^2 - u) + \frac{(2 \sin^2 \theta_W - 1)}{2R_t(l_J) R_s^*(\tilde{\nu}_{mL})} \left( (m_{\tilde{\nu}_{mL}}^2 - t)(m_{\tilde{\nu}_{mL}}^2 - u) + s(m_{\tilde{\nu}_{mL}}^2 - u) \right. \\
& + (m_Z^2 - t)(m_{\tilde{\nu}_{mL}}^2 - t) - \frac{s}{m_Z^2} (m_Z^2 - t)(s - m_{\tilde{\nu}_{mL}}^2 - m_Z^2) \left. \right) + \frac{(2 \sin^2 \theta_W - 1)(\sin^2 \theta_W)}{R_t(l_J) R_u^*(l_J)} \\
& \times \left( (m_{\tilde{\nu}_{mL}}^2 - u)(m_{\tilde{\nu}_{mL}}^2 - t) + s m_{\tilde{\nu}_{mL}}^2 - \frac{1}{M_Z^2} \left( -\frac{(s - m_{\tilde{\nu}_{mL}}^2 - m_Z^2)}{2} ((m_{\tilde{\nu}_{mL}}^2 - u)(m_Z^2 - u) \right. \right. \\
& + (m_{\tilde{\nu}_{mL}}^2 - t)(m_Z^2 - t) - s(s - m_{\tilde{\nu}_{mL}}^2 - m_Z^2)) + (m_Z^2 - u)(m_Z^2 - t)m_{\tilde{\nu}_{mL}}^2 \left. \left. \right) \right], \tag{A.5}
\end{aligned}$$

$$\begin{aligned}
\sum_{pol} |M(\tilde{\nu}_{mL} + \gamma)|^2 &= 2e^2 |\lambda_{mJJ}|^2 ((m_{\tilde{\nu}_{mL}}^2 - t)(m_{\tilde{\nu}_{mL}}^2 - u) - s m_{\nu_m}^2) \left[ \frac{1}{|R_t(l_J)|^2} + \frac{1}{|R_u(l_J)|^2} \right] \\
& + 4e^2 |\lambda_{mJJ}|^2 Re \frac{(m_{\tilde{\nu}_{mL}}^2 - t)(m_{\tilde{\nu}_{mL}}^2 - u)}{R_t(l_J) R_u^*(l_J)}, \tag{A.6}
\end{aligned}$$

where  $Re$  stands for the real part,  $R_s(\tilde{\nu}_i) = s - m_{\tilde{\nu}_i}^2 + im_{\tilde{\nu}} \Gamma_{\tilde{\nu}}$ ,  $R_t(\tilde{\nu}_i) = t - m_{\tilde{\nu}_i}^2$  and  $R_u(\tilde{\nu}_i) = u - m_{\tilde{\nu}_i}^2$ ,  $[s = (k + k')^2, t = (k - p)^2, u = (k - p')^2]$ , with similar definitions applying for the propagator factors  $R_{s,t,u}(l_i, \tilde{l}_i)$ .

## B Formulas for partial decay widths

The formulas for the various two-body decay widths are quoted below.

$$\Gamma(\tilde{\nu} \rightarrow \tilde{\chi}_a^+ + l^-) = \frac{g^2}{16\pi} |V_{a1}|^2 m_{\tilde{\nu}} \left( 1 - \frac{m_{\tilde{\chi}_a}^2}{m_{\tilde{\nu}}^2} \right)^2 \tag{B.1}$$

$$\Gamma(\tilde{\nu} \rightarrow \tilde{\chi}_a^0 + \nu) = \frac{g^2}{32\pi} |N_{a2} - N_{a1} \tan \theta_W|^2 m_{\tilde{\nu}} \left( 1 - \frac{m_{\tilde{\chi}_a}^2}{m_{\tilde{\nu}}^2} \right)^2 \tag{B.2}$$

$$\Gamma(\tilde{l}_L^+ \rightarrow \tilde{\chi}_a^+ \tilde{\nu}) = \frac{g^2}{16\pi} |U_{a1}|^2 m_{\tilde{l}_L} \left( 1 - \frac{m_{\tilde{\chi}_a}^2}{m_{\tilde{l}_L}^2} \right)^2 \tag{B.3}$$

$$\Gamma(\tilde{l}_{[L,R]}^- \rightarrow \tilde{\chi}_a^0 + l^-) = \frac{g^2}{32\pi} [|N_{a2} + N_{a1} \tan \theta_W|^2, |N_{a2} \tan \theta_W|^2] m_{\tilde{l}_H} \left( 1 - \frac{m_{\tilde{\chi}_a}^2}{m_{\tilde{l}_H}^2} \right)^2 \tag{B.4}$$

$$\begin{aligned}
\Gamma(\tilde{\nu}_i(M) \rightarrow l_k^-(m_1) + l_j^+(m_2)) &= \Gamma(\tilde{l}_{jL}^-(M) \rightarrow \bar{\nu}_i(m_1) + l_k^-(m_2)) \\
&= \Gamma(\tilde{l}_{kR}^-(M) \rightarrow \nu_i(m_1) + l_j^-(m_2)) \\
&= \frac{|\lambda_{ijk}|^2}{8\pi} k \left(1 - \frac{m_1^2 + m_2^2}{M^2}\right)
\end{aligned} \tag{B.5}$$

$$\begin{aligned}
\Gamma(\tilde{\chi}_m^\pm(M_\pm) \rightarrow \tilde{\chi}_l^0(M_0) + W^\pm(m_W)) &= \frac{g^2|k|}{16\pi M_\pm^2} \left[ (|O_L|^2 + |O_R|^2) \left( (M_+^2 + M_0^2 - m_W^2) \right. \right. \\
&\quad \left. \left. + \frac{1}{m_W^2} (M_\pm^2 - M_0^2 - m_W^2)(M_\pm^2 - M_0^2 + m_W^2) \right) \right. \\
&\quad \left. - 12M_0 M_\pm \text{Re} \left( O_L O_R^* \right) \right]
\end{aligned} \tag{B.6}$$

$$\begin{aligned}
\Gamma(\tilde{\chi}_a^0 \rightarrow \tilde{f}_{[L,R]} \bar{f}') &= \frac{g^2 M_0}{16\pi} \left(1 - \frac{m_{\tilde{f}}^2}{M_0^2}\right)^2 \\
&\quad [T_3^f N_{a2} - \tan \theta_W (T_3^f - Q^f) N_{a1}]^2, |\tan \theta_W N_{a2}|^2]
\end{aligned} \tag{B.7}$$

$$\Gamma(\tilde{\chi}_a^\pm \rightarrow \tilde{f}_{[T_3^f=-1/2, 1/2]} \bar{f}') = \frac{g^2 M_\pm}{32\pi} \left(1 - \frac{m_{\tilde{f}}^2}{M_\pm^2}\right)^2 [|U_{a1}|^2, |V_{a1}|^2]. \tag{B.8}$$

We use the notations:  $O^L = O_{lm}^L = N_{l2} V_{m1}^* - \frac{1}{\sqrt{2}} N_{l4} V_{m2}^*$ ,  $O^R = O_{lm}^R = N_{l2} U_{m1} + \frac{1}{\sqrt{2}} N_{l3}^* U_{m2}$ ,  $M_\pm = m_{\tilde{\chi}_a^\pm}$ ,  $M_0 = m_{\tilde{\chi}_a^0}$  and  $k = \lambda^{\frac{1}{2}}(M^2, m_1^2, m_2^2)/2M$  with  $\lambda(a, b, c) = a^2 + b^2 + c^2 + ab + bc + ac$ . The notations,  $T_3^f$ ,  $Q^f$ , stand for the third component of the  $SU(2)_L$  group and the electric charge of the fermion  $f$ . We have omitted the higgsino components of the inos. We shall use the simplified formulas for the RPC three-body decays,  $\tilde{\chi}_m^- \rightarrow \tilde{\chi}_l^0 + l\bar{\nu}$ ,  $q\bar{q}$ , obtained by neglecting the three-momenta in the W and  $\tilde{l}$  propagators, as quoted in [54]. We have set in these formulas, the flavor and color parameters to,  $N_f = 2$ ,  $N_c = 3$  for quarks and  $N_f = 3$ ,  $N_c = 1$  for leptons. The formulas for the spin summed amplitudes of the RPV decays  $\tilde{\chi}_a^- \rightarrow \bar{\nu}_i \bar{\nu}_j l_k^-$ ,  $\tilde{\chi}_a^- \rightarrow l_k^+ l_j^- l_i^-$ , associated to the coupling constants  $\lambda_{ijk}$ , were first derived in [15] (see the appendix). The integrated decay rates are given by familiar formulas [47] involving twofold integrals over the final state three-body phase space. If we neglect the final particles masses, an analytic formula can be derived for the integral giving the contributions to the charginos partial rates associated with the gauginos components only (neglecting the higgsino components contribution). For completeness, we display the final results:

$$\begin{aligned}
\Gamma(\tilde{\chi}_a^-) &= M_{\tilde{\chi}_a^-} \frac{g^2 X_{a1}^2 |\lambda_{ijk}|^2}{128\pi^3} \left[ \frac{1}{8} \left( -5 + 6\mu_i + (2 - 8\mu_i + 6\mu_i^2) \log\left(1 - \frac{1}{\mu_i}\right) \right. \right. \\
&\quad \left. \left. - 5 + 6\mu_j + (2 - 8\mu_j + 6\mu_j^2) \log\left(1 - \frac{1}{\mu_j}\right) \right) \right. \\
&\quad + \frac{1}{2} \left( \mu_i + \mu_j - \frac{1}{2} + (\mu_i^2 - \mu_i) \log\left(1 - \frac{1}{\mu_i}\right) + (\mu_j^2 - \mu_j) \log\left(1 - \frac{1}{\mu_j}\right) \right. \\
&\quad \left. - \mu_i \mu_j \log\left(1 - \frac{1}{\mu_i}\right) \log\left(\frac{\mu_i + \mu_j - 1}{\mu_j}\right) \right. \\
&\quad \left. - \mu_i \mu_j \log\left(1 - \frac{1}{\mu_j}\right) \log\left(\frac{\mu_i + \mu_j - 1}{\mu_i}\right) \right. \\
&\quad \left. + \mu_i \mu_j \left[ Sp\left(\frac{\mu_i}{\mu_j}\right) + Sp\left(\frac{\mu_j}{\mu_i}\right) - Sp\left(\frac{1 - \mu_i}{\mu_j}\right) - Sp\left(\frac{1 - \mu_j}{\mu_i}\right) \right] \right],
\end{aligned} \tag{B.9}$$

where  $Sp(x) = Polylog(x) = Li_2(x)$  is the Spence or Polylog function. We use the notations  $\mu_\alpha = m_{\tilde{\nu}_\alpha}^2 / M_{\tilde{\chi}_a^-}^2$ ,  $[\alpha = i, j]$ ,  $X_{a1} = U_{a1}$  for the decay  $\tilde{\chi}_a^- \rightarrow l_k^+ l_j^- l_i^-$ , and  $\mu_\alpha = m_{l_\alpha}^2 / M_{\tilde{\chi}_a^-}^2$ ,  $[\alpha = i, j]$ ,  $X_{a1} = V_{a1}$  for the decay  $\tilde{\chi}_a^- \rightarrow \bar{\nu}_i \bar{\nu}_j l_k^-$ .

## References

- [1] S. Dimopoulos and L. J. Hall, Phys. Lett. **B207** (1988) 210
- [2] V. Barger, G.F. Giudice and T. Han, Phys. Rev. **D40** (1989) 2987
- [3] H. Dreiner and G.G. Ross, Nucl. Phys. **B365** (1991) 597
- [4] R. Barbieri, D. E. Brahm, L. J. Hall and S. D. H. Hsu, Phys. Lett. **B238** (1990) 86
- [5] D. E. Brahm and L. J. Hall, Phys. Rev. **D40** (1989) 2449
- [6] S. Lola and J. Mc Curry, Nucl. Phys. **B381** (1992) 559
- [7] H. Dreiner and R. J. N. Phillips, Nucl. Phys. **B367** (1991) 591
- [8] Opal Coll., Phys. Lett., **B313** (1993) 333
- [9] Aleph Coll., Phys. Lett., **B349** (1995) 238
- [10] D. P. Roy, Phys. Lett., **B283** (1992) 270
- [11] Aleph Coll., Phys. Lett., **B384** (1996) 461
- [12] Delphi Coll., Y. Arnoud et al., 20 July 1997, DELPHI 97-119, CONF 101, Hep'97
- [13] Aleph Coll., R. Barate et al., Eur. Phys. J., **C4** (1998) 433
- [14] D. Buskulic et al., Aleph Coll., Z. Phys. **C71** (1996) 179; F. Ragusa, for the Aleph Coll., talk at the LEPC Meeting, November 19, 1996
- [15] H. Dreiner, S. Lola and P. Morawitz, Phys. Lett. **B389** (1996) 62
- [16] D. Choudhury and D. P. Roy, Phys. Rev. **D54** (1996) 6797; D. K. Ghosh, R. M. Godbole and S. Raychaudhuri, Z. Phys. **C 75** (1997) 357
- [17] P. Chankowski, D. Choudhuri and S. Pokorski, Phys. Lett. **B389** (1996) 677
- [18] A. K. Grant, R. D. Peccei, T. Vettore and K. Wang, Phys. Lett. **B379** (1996) 272
- [19] G. R. Farrar, Phys. Rev. Lett. **76** (1996) 4115
- [20] M. Carena, G. F. Giudice, S. Lola, C. E. M. Wagner, Phys. Lett. **B395** (1997) 225
- [21] V. Barger, W.-Y. Keung and R. J. N. Phillips, Phys. Lett. **B364** (1995) 27
- [22] R. Barate et al., (Aleph Coll.) Phys. Lett. **B420** (1998) 196; K. Ackerstaff et al., (Opal Coll.) Phys. Lett. **B429** (1998) 399
- [23] J. Butterworth and H. Dreiner, Nucl. Phys. **B397** (1993) 3
- [24] E. Perez, Y. Sirois and H. Dreiner, hep-ph/9703444
- [25] H1 Coll., S. Aid et al, Z.Phys. **C71**, 211 (1996)
- [26] G. Bhattacharyya, Invited talk presented at 'Beyond the Desert', Castle Ringberg, Tegemsee, Germany, 8-14 June 1997; Susy '96, Nucl. Phys. B (Proc. Suppl.) **52A** (1997) 83
- [27] S. Dimopoulos, R. Esmailzadeh, L.J. Hall, J. Merlo and G.D. Starkman, Phys. Rev. **D41** (1990) 2099
- [28] A. Datta, J. M. Yang, B.-L. Young and X. Zhang, Phys. Rev **D 56** (1997) 3107
- [29] R. J. Oakes, K. Whisnant, J. M. Yang, B.-L. Young and X. Zhang, Phys. Rev. **D 57** (1998) 534
- [30] J. Erler, J.L. Feng and N. Polonsky, Phys. Rev. Lett. **78** (1997) 3063

- [31] J. Kalinowski, R. R ueckl, H. Spiesberger and P.M. Zerwas, Phys. Lett. **B406** (1997) 314
- [32] J. Kalinowski, R. R ueckl, H. Spiesberger and P.M. Zerwas, Phys. Lett. **B414** (1997) 297
- [33] J. Breitweg and al, Zeus Coll., DESY 97-025 and Z. Phys. **C74** (1997) 207
- [34] C. Adloff and al, H1 Coll., DESY 97-024 and Z. Phys. **C74** (1997) 191
- [35] D. Choudhury and S. Raychaudhuri, Phys.Lett. **B401**, 54 (1997); G. Altarelli, J. Ellis, G. F. Giudice, S. Lola, M. L. Mangano, Nucl.Phys. **B506**, 3 (1997); H. Dreiner and P. Morawitz, Nucl.Phys. **B503**, 55 (1997); J. Kalinowski, R. R ueckl, H. Spiesberger and P.M. Zerwas, Z.Phys. **C74**, 595 (1997); T. Kon and T. Kobayashi, Phys.Lett. **B409**, 265 (1997)
- [36] H. Murayama and M. E. Peskin, Ann. Rev. Nucl. Part. Science **46** (1996) 533
- [37] H.Dreiner and S. Lola, published in “ Munich /Annecy/Hamburg 1991, Proceedings,  $e^+e^-$  collisions at 500 GeV”; “Searches for New Physics”, contribution to the LEPII workshop, 1996, hep-ph/9602207
- [38] E. Accomando et al., “Physics with  $e^+e^-$  Linear Colliders”, DESY-97-100, hep-ph/9705442
- [39] B.C. Allanach, H. Dreiner, P. Morawitz and M.D. Williams, hep-ph/9708495
- [40] SUSYGEN 2.2 - A Monte Carlo Event Generator for MSSM Sparticle Production at  $e^+e^-$  colliders, S. Katsanevas and P. Morawitz, IC/HEP/97-5, IFAE-UAB/97-01, LYCEN 9744, submitted to Physics Communications, location: <http://lyohp5.in2p3.fr/delphi/katsan/susygen.html>
- [41] S. Katsanevas and P. Morawitz, IC/HEP/97-5, IFAE-UAB/97-01, LYCEN 9744, submitted to Physics Communications
- [42] D. Choudhury and D. P. Roy, Phys. Lett. **B378** (1996) 153
- [43] S. Dawson, Nucl. Phys. **B261** (1985) 297
- [44] M. Drees and M. M. Nojiri, Nucl. Phys. **B369** (1992) 54
- [45] V. Barger, M. S. Berger and P. Ohmann, Phys. Rev. **D49** (1994) 4908
- [46] M. Carena, M. Olechowski, S. Pokorski and C. E. M. Wagner, Nucl. Phys. **B419** (1994) 213
- [47] Particle Data Group, R. M. Barnett et al., Phys. Rev. **D54** (1996) 1
- [48] H.E. Haber and G.L. Kane, Phys. Rep. **117** (1985) 175
- [49] J. A. Bagger, Nucl. Phys. B (Proc. Suppl.) **62** (1998) 23
- [50] V. Barger, M. S. Berger, J. F. Gunion and T. Han, MADPHY-96-939, Nucl. Phys. (Proc. Suppl.) **51A** (1996) 13; V. Barger, MADPHY-98-1038, hep-ph/9802355
- [51] B. Grinstein, J. Polchinski and M. B. Wise, Phys. Lett. **B130** (1983) 285
- [52] S. Dimopoulos, S. Thomas and J. D. Wells, Nucl. Phys. **B488** (1997) 39
- [53] K. Fujii, Susy’95, eds. I. Antoniadis and H. Videau (Editions Frontieres, Gif-sur-Yvette,1996) 123
- [54] J. L. Feng and M. J. Strassler, Phys. Rev. **D51** (1995) 4661